

1 **Heterogeneous reaction of peroxyacetic acid and hydrogen**
2 **peroxide on ambient aerosol particles under dry and humid**
3 **conditions: kinetics, mechanism and implications**

4 **Q. Q. Wu¹, L. B. Huang¹, H. Liang¹, Y. Zhao^{1,*}, D. Huang^{1,**}, and Z. M. Chen¹**

5 ¹State Key Laboratory of Environmental Simulation and Pollution Control, College
6 of Environmental Sciences and Engineering, Peking University, Beijing 100871,
7 China

8 * now at: Department of Chemistry, University of California, Irvine, CA 92697, USA

9 ** now at: Department of Earth Sciences, Zhejiang University, Hangzhou, Zhejiang
10 Province 310027, China

11 *Correspondence to:* Z. M. Chen (zmchen@pku.edu.cn)

12

13 **Abstract.** Hydrogen peroxide (H₂O₂) and organic peroxides play important roles in
14 the cycle of oxidants and the formation of secondary aerosols in the atmosphere.
15 Recent field observations have suggested that the budget of peroxyacetic acid (PAA,
16 CH₃C(O)OOH) is potentially related to the aerosol-phase processes, especially to
17 secondary aerosol formation. Here we present the first laboratory measurements of
18 the uptake coefficient of gaseous PAA and H₂O₂ onto ambient fine particulate matter
19 (PM_{2.5}) as a function of relative humidity (RH) at 298 K. The results show that the
20 PM_{2.5}, which was collected in an urban area, can take up PAA and H₂O₂ at the uptake
21 coefficient (γ) of 10⁻⁴, and both γ_{PAA} and $\gamma_{\text{H}_2\text{O}_2}$ increase with increasing RH. The
22 value of γ_{PAA} at 90% RH is 5.4±1.9 times of that at 3% RH whereas $\gamma_{\text{H}_2\text{O}_2}$ at 90% RH
23 is 2.4±0.5 times of that at 3% RH, which suggests that PAA is more sensitive to the
24 RH variation than H₂O₂ is. Considering the larger Henry's law constant of H₂O₂ than
25 that of PAA, the smaller RH sensitivity of H₂O₂ uptake coefficient suggests that the
26 enhanced uptake of peroxide compounds on PM_{2.5} under humid conditions is

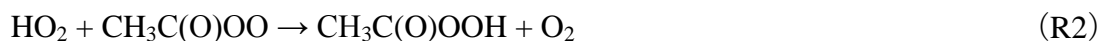
27 dominated by chemical processes rather than dissolution. Considering that mineral
28 dust is one of the main components of PM_{2.5} in Beijing, we also determined the
29 uptake coefficients of gaseous PAA and H₂O₂ on authentic Asian Dust Storm (ADS)
30 and Arizona Test Dust (ATD) particles. Compared to ambient PM_{2.5}, ADS shows a
31 similar γ value and RH dependence in its uptake coefficient for PAA and H₂O₂, while
32 ATD gives a negative dependence on RH. The present study indicates that in
33 addition to the mineral dust in PM_{2.5}, other components (e.g., inorganic soluble salts)
34 are also important to the uptake of peroxide compounds. When the heterogeneous
35 reaction of PAA on PM_{2.5} is considered, its atmospheric lifetime is estimated to be
36 3.0 h on haze days and 7.1 h on non-haze days, values which are in good agreement
37 with the field observations.

38 **1 Introduction**

39 Peroxide compounds, including hydrogen peroxide (H₂O₂) and organic peroxides,
40 play an important role in the chemistry of the atmosphere, because they serve as
41 oxidants for the conversion of S(IV) to S(VI) in the atmospheric aqueous phase,
42 resulting in the formation of sulfate aerosol (Calvert et al., 1985; Lind et al., 1987;
43 Stein and Saylor, 2012). Peroxide species also serve as a reservoir for HO_x (OH and
44 HO₂) radicals (Wallington and Japar, 1990; Vaghjiani et al., 1990; Atkinson et al.,
45 1992; Ravetta et al., 2001) and RO_x (RO and RO₂) radicals (Lightfoot et al., 1991;
46 Reeves and Penkett, 2003). Moreover, recent laboratory studies have indicated that
47 peroxide compounds, especially organic peroxides, significantly contribute to the
48 formation and aging of secondary organic aerosols (SOA) (Claeys et al., 2004;
49 Docherty et al., 2005; Surratt et al., 2006; Paulot et al., 2009; Huang et al., 2013; Xu
50 et al., 2014; Zhao et al., 2015).

51 The peroxide compounds are mainly produced by the bimolecular reaction of
52 HO₂ and RO₂ radicals (e.g., R1 and R2), and their minor sources include the
53 ozonolysis of alkenes and biomass burning (Lee et al., 2000).





54 Their traditional removal pathways include reacting with OH radicals, photolysis
55 and deposition (Lee et al., 2000). Recent studies have combined field and model data
56 to ascertain the importance of heterogeneous loss. For example, de Reus et al. (2005)
57 have demonstrated that in the subtropical island, the concentration of gaseous H₂O₂
58 was largely overestimated by a standard gas-phase chemical mechanism. When the
59 heterogeneous uptake of H₂O₂ and/or HO₂ radicals on the surface of aerosols was
60 accounted for in the model, the observed and modeled values were in better
61 agreement. In addition, a series of laboratory studies have addressed the importance
62 of the heterogeneous reaction of H₂O₂ on model or authentic mineral dust particles
63 (Pradhan et al., 2010a; Pradhan et al., 2010b; Wang et al., 2011; Zhao et al., 2011a;
64 Zhao et al., 2011b; Romanias et al., 2012; Zhou et al., 2012; Romanias et al., 2013;
65 Zhao et al., 2013; El Zein et al., 2014). For example, Pradhan et al. (2010a) have
66 indicated that the heterogeneous reaction of H₂O₂ on dust aerosols could compete
67 with its photolysis and significantly affect HO_x radical budget. Romanias et al. (2012,
68 2013) have confirmed that the heterogeneous reaction of H₂O₂ on mineral dust had
69 an important effect on the fate of HO_x radicals. El Zein et al. (2014) also suggested
70 that the lifetime of H₂O₂ removed by heterogeneous reaction was comparable with its
71 photolysis on severe dust storm period. Our recent study has indicated that H₂O₂
72 could enhance the uptake of oxygenated volatile organic compounds (OVOCs) onto
73 the surface of mineral dust particles (Zhao et al., 2014).

74 To the best of our knowledge, to date, there has been no laboratory experimental
75 evidence for the importance of the heterogeneous reactions of organic peroxides in
76 the atmosphere. As an important organic peroxide, peroxyacetic acid (PAA,
77 CH₃C(O)OOH) has been frequently detected over both rural and urban areas (Lee et
78 al., 1995; Hua et al., 2008; He et al., 2010; Zhang et al., 2010; Liang et al., 2013;
79 Phillips et al., 2013). The typical concentration of PAA is comparable to that of H₂O₂,
80 i.e., several tens to hundreds of pptv in summer, and the maximum concentration
81 surpasses 1 ppbv over the Mazhuang, a rural site in Shandong Province, China

82 (Zhang et al., 2010) and the boreal forest (Phillips et al., 2013). Our field observation
83 results have suggested that heterogeneous reactions on aerosol particles might be an
84 important removal pathway for PAA in the atmosphere (Zhang et al., 2010; Liang et
85 al., 2013). Therefore, we use PAA as representative organic peroxide to investigate
86 the kinetics and mechanisms of its heterogeneous reactions on ambient PM_{2.5} as well
87 as mineral dust particles over a wide range of relative humidities (3–90%). We also
88 estimate the contribution of heterogeneous reactions to PAA budget in the
89 atmosphere. As a comparison, we investigate the kinetics of H₂O₂ uptake on PM_{2.5}.

90 **2 Experimental**

91 **2.1 Reagents and materials**

92 Hydrogen peroxide (H₂O₂, Alfa Aesar, 35% water solution), acetic acid (CH₃COOH,
93 Xilong Chemical Co., LTD, 99.8%), and sulfuric acid (H₂SO₄, Beijing Chemical
94 Plant, 95–98%) were used to prepare the PAA solutions. *Ortho*-Phosphoric acid
95 (H₃PO₄, Fluka, 85%); hemin (Sigma, ≥ 98%), *p*-hydroxyphenylacetic acid (POPHA,
96 Alfa Aesar, 99%), ammonia solution (NH₃·H₂O, Beijing Tongguang Fine Chemicals
97 Company, 25.0–28.0%), ammonium chloride (NH₄Cl, Beijing Chemical Works, ≥
98 99.5%), N₂ gas (≥ 99.999%, Beijing Haikeyuanchang Practical Gas Company
99 Limited, Beijing, China), O₂ gas (≥ 99.999%, Beijing Haikeyuanchang Practical Gas
100 Company Limited, Beijing, China) and polytetrafluoroethylene (PTFE) filter
101 membrane (Whatman Inc., 47 mm in diameter) were also used in the experiments.
102 Asian Dust Storm particles (ADS particles, the BET surface area is 6.1 m² g⁻¹) and
103 Arizona Test Dust particles (ATD particles, Al Ultrafine test dust, Powder
104 Technology, the BET surface area is 16.5 m² g⁻¹) were used. ADS particles were
105 collected at PKU campus in April 17, 2006 after a strong sand storm. The ADS
106 particles deposited on a glass plate and then were collected and kept in a glass bottle.

107 **2.2 Apparatus and procedures**

108 **2.2.1 Generation of gaseous PAA and H₂O₂**

109 PAA aqueous solution was synthesized by mixing H₂O₂ aqueous solution with acetic

110 acid aqueous solution, using H_2SO_4 as a catalyst (Dul'neva and Moskvin, 2005;
111 Zhao et al., 2007). The mixing aqueous solution was kept in the dark for 24 h at
112 room temperature to make sure PAA reached its maximum balanced concentration.
113 The PAA concentration in this primary solution (S1) was 1.3 M. The solution was
114 stored at 277 K in the dark before use. At the beginning of every experiment, a PAA
115 solution (S2) (4×10^{-5} M) was prepared by diluting S1 with ultrapure water and then
116 100 mL S2 was added into a 1 L bubbler. The S2 in the bubbler, kept in a 277 K
117 water bath in the dark, was bubbled by a N_2 flow at a rate of 70 mL min^{-1} to generate
118 gaseous PAA. The PAA-containing N_2 flow was then mixed with an O_2 flow and
119 water vapor flow generated by another bubbler. The resulting gas mixture (reactant
120 gas) was introduced into the filter-based flow reactor as described in Section 2.2.3. A
121 H_3PO_4 solution (5×10^{-3} M) was used to scrub gaseous peroxide in a glass scrubbing
122 coil. The collection efficiency was 85% for PAA and 100% for H_2O_2 at 277 K (Hua
123 et al., 2008; Liang et al., 2013). The peroxide-containing scrubbing solution was
124 analyzed immediately by an online high-performance liquid chromatography (HPLC,
125 Agilent 1200). The method is described in detailed in Section 2.3. The concentration
126 of PAA was 300 ± 30 pptv in the gas mixture. To ensure a constant concentration of
127 gaseous PAA, the bubbling solution of PAA was renewed every day. The generation
128 of gaseous H_2O_2 was similar to that of PAA. The concentration of the bubbling
129 solution of H_2O_2 was 1.14×10^{-3} M. The resulting H_2O_2 concentration was 510 ± 40
130 pptv in the gas mixture.

131 **2.2.2 Preparation of particle-loaded filters**

132 The $\text{PM}_{2.5}$ samples were collected on the roof of a six-story teaching building (26 m
133 above the ground) at the campus of Peking University (PKU), Beijing, China. PKU
134 is located in the northwest downtown area, with two major traffic arteries passing by.
135 An ambient particulate sampler (TH-16A, Wuhan Tianhong Instruments Co., Ltd)
136 was used to collect the $\text{PM}_{2.5}$ particles on the PTFE filters with four parallel channels
137 operating simultaneously and the sampling flow of each channel was 16.7 standard L
138 min^{-1} . The $\text{PM}_{2.5}$ samples were collected for 6 days, from 31 July 2014 to 6 August

139 2014. Sampling was conducted twice a day for 11.5 h each time (daytime, 9:00–
140 20:30 LT; nighttime, 21:00–08:30 LT). During the sampling period, 31 July to 3
141 August were haze days and 3 August to 5 August were non-haze days. Haze is
142 caused by a large amount of fine particles (e.g., dust, smoke, salt) with RH less than
143 90% and makes the visibility less than 10 km (Li, 2010). Here, we differentiated
144 non-haze days from haze days based on two criteria. One was the visibility of a
145 mountain (by eye) which is about 10 km away from the sampling site. The other was
146 the national ambient air quality standard grade II in China, i.e., average PM_{2.5} mass
147 concentration of lower than 75 μg m⁻³. The PM_{2.5} particle-loaded filters were sealed
148 and kept at 255 K before use. ADS and ATD particles were separately used to
149 prepare the mineral dust particle-loaded filters. Mineral dust particles were
150 resuspended using a custom-built resuspension apparatus and then collected on the
151 PTFE filters. The resuspension apparatus consists of three parts, i.e., glass inlet,
152 stainless filter holder and vacuum pump. First, we put a known amount of mineral
153 dust particles into the glass inlet and then turned off the inlet. Secondly, we turned on
154 the vacuum pump and a negative pressure was then formed in this resuspension
155 system. Finally, we turned on the inlet, and the particles were resuspended with the
156 help of airflow and collected onto the filter. To compare the experimental results for
157 PM_{2.5} sampled on non-haze and haze days, the mass of ADS or ATD on the filter was
158 carefully controlled at 0.3 mg and 1.3 mg for the lower and higher particle mass,
159 respectively.

160 **2.2.3 Uptake experiments**

161 A filter based flow reactor was used to measure the uptake coefficients of gaseous
162 peroxides on aerosol particles. The schematic of this experimental apparatus is
163 shown in Figure 1. The reactor is composed of two perfluoroalkoxy resin filter
164 holders (Savillex Corporation) connected in parallel. One reactor contains a blank
165 PTFE filter, and the other contains a particle-loaded filter. The tubing system is made
166 of Teflon tubes. The peroxide containing gas mixture (20% O₂ + 80% N₂) was used
167 at a flow rate of 2.7 standard L min⁻¹ and was introduced into the blank reactor or the

168 particle-loaded reactor via two unreactive stainless steel valves. After exiting the
 169 reactor, the peroxide containing gas was directed into a glass scrubbing coil in a
 170 277 ± 0.1 K water bath, in which a H_3PO_4 solution (5×10^{-3} M) was used as the eluent
 171 to scrub the peroxide at a rate of 0.2 mL min^{-1} . The same particle-loaded filter was
 172 used to measure the uptake coefficient at a continuously increasing RH ranging from
 173 3% to 90% and then the measurement was repeated in reverse, at a decreasing RH
 174 from 90% to 3%. We have compared the uptake coefficients of PAA on the exposed
 175 $\text{PM}_{2.5}$ filter which has been used in the PAA uptake experiments and the unexposed
 176 $\text{PM}_{2.5}$ filter which has not been used for any experiments at 60% RH, and no obvious
 177 difference was observed between the two uptake coefficients (Table 1). Therefore,
 178 we think the reuse of the filter for experiments at different RH has no significant
 179 effect on the results.

180 The uptake experiment at a certain RH took 2 h for PAA and 1 h for H_2O_2 ;
 181 including the time for the balance of peroxide on blank filter and particles-loaded
 182 filter. The balance concentrations of PAA/ H_2O_2 have been detected at least for three
 183 times. Then the RH was directly changed to another RH without any treatment for
 184 the filter samples. All the experiments were conducted at 298 ± 2 K, ambient pressure
 185 and in the dark.

186 The uptake coefficients of gaseous peroxide can be calculated using the following
 187 equations (Molina et al., 1996; Zhao et al., 2010):

$$\gamma = \frac{d\{C\}/dt}{Z} \quad (1)$$

$$Z = \frac{1}{4} \omega A_{\text{es}} [C] \quad (2)$$

$$\omega = \sqrt{\frac{8RT}{\pi M_x}} \quad (3)$$

188 where $\{C\}$ is the total uptake of gaseous peroxide by particle surfaces, molecules; Z
 189 is the collision frequency, molecules s^{-1} ; $[C]$ is the number concentration of gaseous
 190 peroxide, molecules m^{-3} ; ω is the mean molecular speed, m s^{-1} ; R is the universal gas

191 constant, $\text{kg m}^2 \text{s}^{-2} \text{mol}^{-1} \text{K}^{-1}$; T is the temperature, K; A_{es} is the effective surface area
192 of particles, m^2 ; M_x is the molecular weight, kg mol^{-1} . The uptake onto the particles
193 is equal to the loss of the gaseous reactant and this gas phase loss can be calculated
194 by the difference between the reactant concentrations at the inlet and outlet of the
195 reactor. Here, we define the fractional loss of the reactant (Lf) as Eq. (4):

$$\text{Lf} = \frac{[C]_{\text{in}} - [C]_{\text{out}}}{[C]_{\text{in}}} \quad (4)$$

196 where $[C]_{\text{in}}$ and $[C]_{\text{out}}$ is the concentration of the reactant at the inlet and outlet of the
197 reactor, molecules m^{-3} , respectively. Since no obvious uptake of peroxide on the
198 blank filter occurred, the reactant concentration at the outlet of the blank reactor can
199 be treated as the initial concentration at the inlet of the reactor for the uptake on
200 aerosols. Therefore, Eq. (1) can be expressed as Eq. (5):

$$\gamma = \frac{4 \times \text{Lf} \times V_g}{\omega A_{\text{es}}} \quad (5)$$

201 where V_g is the flow rate of the reactant containing gas, $\text{m}^3 \text{s}^{-1}$. The values of γ on
202 $\text{PM}_{2.5}$, ADS and ATD particles in the next test are calculated by the A_{es} estimated in
203 Section 2.4.

204 **2.3 Analysis of Peroxides, Soluble Species and Elements**

205 Peroxide compounds were measured by HPLC coupled with a post-column
206 derivatization module. The length of the column is 150 mm (Alltima AQ 5 μ). The
207 details of this method have been reported in our previous study (Hua et al., 2008).
208 Briefly, this method is based on the determination of the fluorescent dimer produced
209 by the reaction of POPHA and peroxides with the catalysis of hemin. The HPLC
210 mobile phase was H_3PO_4 solution (pH=3.5) at a flow rate of 0.5 mL min^{-1} . The
211 formed fluorescent dimer was analyzed by a fluorescence detector. The time of
212 collecting a chromatogram was 10 min for PAA and 5.0 min for H_2O_2 . The retention
213 times of PAA and H_2O_2 were 8.9 min and 4.0 min, respectively.

214 We used ultrasonic method to extract the soluble compounds in particles samples.
215 Each sample was exposed to ultrasonic treatment in ice water with 10 mL Milli-Q
216 water for 30 min. The extracted soluble compounds were measured by ion
217 chromatography (IC, Dionex ICS2000 and ICS2500). The analytical column for
218 cation and anion was Dionex CS 12A and Dionex AS 11, respectively. Here, the
219 measured compounds include eight inorganic ions (i.e., K^+ , Ca^{2+} , Na^+ , Mg^{2+} , NH_4^+ ,
220 Cl^- , NO_3^- and SO_4^{2-}) and four organic acids (i.e., formic acid, acetic acid, pyruvic
221 acid and oxalic acid).

222 We used acid digestion to extract elements in particles through microwave
223 digestion system (CEM MARS, USA). Elements in the extractions were measured
224 by inductively coupled plasma mass spectroscopy (ICP-MS, Thermo X series). The
225 measured elements include Mg, Al, P, Ca, Ti, V, Cr, Mn, Fe, Co, Ni, Cu, Zn, As, Se,
226 Mo, Cd, Ba, Tl, Pb, Th and U.

227 **2.4 Estimation of effective surface area**

228 The effective surface area (A_{es}) is a key factor in the uptake of a specific compound
229 from the gas phase onto aerosol particles. The uptake coefficient (γ) estimated by the
230 geometric filter surface area (A_{gs}) is several orders of magnitude higher than that by
231 the Brunauer-Emmett-Teller (BET) surface area (Shen et al., 2013). To date,
232 accurate estimation of A_{es} of the particle sample has been a challenge for the
233 determination of γ . Bedjanian et al. (2013) have measured the uptake of HO_2 radicals
234 on ATD particles and showed a pseudo-logarithmic relationship between the uptake
235 and the particle mass. In the present study, ambient particles were loaded on the
236 filter in an agglomerated state, extremely different from their status in the
237 atmosphere, where they are highly dispersed. Obviously, neither the geometric
238 surface area nor the BET surface area can represent the A_{es} of the ambient particle
239 samples on the filter. Here we estimated A_{es} by investigating the relationship between
240 the uptake and loaded particle mass. Eq. (5) shows that the fractional loss (L_f) of a
241 specific gaseous reactant due to the uptake of the filter-loaded particles was directly
242 proportional to A_{es} . The value of A_{es} should depend on the loaded particle mass.

243 Therefore, we used the relationship between Lf and particle mass (M_a) to estimate
 244 the value of A_{es} . Figure 2 shows the relationship between the Lf of gaseous PAA
 245 versus the loaded particle mass. Although Lf appeared to have a linear relationship
 246 with particle mass in the low particle mass region, it generally fitted with the
 247 logarithmic function of particle mass, with a correlation coefficient $r=0.88$. This
 248 empirical logarithmic relationship is given in Eqs. (6) to (8):

$$\text{For PM}_{2.5} \quad Lf=0.15 \times \ln(M_a) + 0.47 \quad (6)$$

$$\text{For ADS} \quad Lf=0.099 \times \ln(M_a) + 0.26 \quad (7)$$

$$\text{For ATD} \quad Lf=0.058 \times \ln(M_a) + 0.20 \quad (8)$$

249 where M_a is the mass of the particles, mg. The mass used for measuring the Lf of
 250 ADS is 0.18, 0.37, 0.81, 1.05, 1.16, 1.63, 1.86 and 2.46 mg, respectively. The mass
 251 for measuring the Lf of ATD is 0.27, 0.48, 0.83, 1.07, 1.36, 1.58, 1.76, 2.02, 2.57 and
 252 3.00 mg, respectively. In the low particle mass region, the particles were highly
 253 dispersed on the filter and A_{es} increased rapidly with increasing particle mass; in high
 254 particle mass region, particles highly overlapped and agglomerated with each other
 255 on the filter, and A_{es} was closer to A_{gs} (12.43 cm^2). Here, we assume that there exists
 256 a critical particle mass ($M_{a,c}$) for which A_{es} is equal to A_{gs} . When the particle mass is
 257 greater than $M_{a,c}$, A_{es} tends to be constant, i.e., the A_{gs} . For $M_{a,c}$, the corresponding
 258 fractional loss of PAA is Lf_c . We used an iterative method to determine $M_{a,c}$. The
 259 termination criterion of this iterative method was the relative error (R_{el}) of Lf_c
 260 towards the average of all the Lf values (\bar{Lf}) which were larger than Lf_c and the
 261 calculation method was expressed in Eq. (9). Here, we set R_{el} as 5% to terminate the
 262 iteration. The procedure of iteration was as follows: (i) start $M_{a,c}$ with 0.10 mg; (ii)
 263 calculate a series values of Lf by inputting a range of M_a (0.01 to 2.00 mg) into Eq.
 264 (6); (iii) calculate R_{el} by the calculated values of Lf and Eq. (9); (iv) if R_{el} is larger
 265 than 5%, reset $M_{a,c}$ with an added mass of 0.01 mg (i.e., 0.11 mg); (v) repeat steps
 266 (ii-iv) until R_{el} is less than 5%, and then obtain the expected $M_{a,c}$ and Lf_c . The
 267 calculated Lf_c was 4.89×10^{-1} , which was similar to the experimental result in Fig. 2.,
 268 i.e., 4.90×10^{-1} . Based on the directly proportional relationship between A_{es} and Lf,

269 A_{es} can be expressed in Eq. (10).

$$R_{el} = \frac{Lf_c}{Lf} \quad (9)$$

$$A_{es} = \frac{A_{gs}}{Lf_c} \times Lf \quad (10)$$

270 The estimation of A_{es} for filter-loaded $PM_{2.5}$, ADS and ATD particles can be
271 expressed as the respective logarithmic functions in Eqs. (11) to (13):

$$\text{For } PM_{2.5} \quad A_{es} = 3.75 \times \ln(M_a) + 12.0 \quad (11)$$

$$\text{For ADS} \quad A_{es} = 3.66 \times \ln(M_a) + 9.59 \quad (12)$$

$$\text{For ATD} \quad A_{es} = 3.01 \times \ln(M_a) + 10.3 \quad (13)$$

272 where M_a represents the filter-loaded particle mass, mg; A_{es} represents the effective
273 surface area of particles, cm^2 . The mass of the filter-loaded $PM_{2.5}$ and the estimated
274 A_{es} values are listed in Table 2. A_{es} for $PM_{2.5}$ changes with the particle mass, ranging
275 from 3.2–13.8 cm^2 ; A_{es} for ADS is 6.1 cm^2 and 10.9 cm^2 , respectively; A_{es} for ATD is
276 6.4 cm^2 and 11.2 cm^2 , respectively. The uptake coefficients on $PM_{2.5}$ particles, ADS
277 and ATD particles below are all calculated with these A_{es} values.

278 3. Results and discussion

279 3.1 Uptake of PAA and H_2O_2 on $PM_{2.5}$

280 The uptake coefficient of PAA (γ_{PAA}) on $PM_{2.5}$ particles was measured over a wide
281 range of RH (3–90%). Figure 3 shows the γ_{PAA} profile on $PM_{2.5}$ with respect to
282 increasing/decreasing RH. γ_{PAA} increases with increasing RH on both daytime and
283 nighttime $PM_{2.5}$ samples. The values of γ_{PAA} on nighttime $PM_{2.5}$ samples are similar
284 to those on daytime $PM_{2.5}$ samples. Additionally, although the mass of $PM_{2.5}$
285 collected on a haze day is significantly different from that on a non-haze day, the
286 γ_{PAA} values are similar under these two different weather conditions (Table 3). In
287 general, γ_{PAA} rises from $(0.89 \pm 0.26) \times 10^{-4}$ at 3% RH to $(4.41 \pm 0.92) \times 10^{-4}$ at 90% RH.
288 Table 3 also lists the lower limit of γ_{PAA} on $PM_{2.5}$, which are calculated using the
289 total surface area of the particles using size distribution (see the details in Section 4,

290 Eq. 21 and Eq. 22). The lower limit is on the order of 10^{-6} – 10^{-5} . The empirical
 291 equation of γ_{PAA} plotted against water activity ($a_{\text{H}_2\text{O}}$; here, $a_{\text{H}_2\text{O}}=\text{RH}/100$) can be
 292 expressed as Eq. (14) and the measured and modelled γ_{PAA} on $\text{PM}_{2.5}$ are shown in
 293 Fig. 4.

$$\gamma_{\text{PAA}} = \frac{4.94 \times 10^{-5}}{1 - 0.91 \times a_{\text{H}_2\text{O}}^{0.21}} \quad (14)$$

294 We also determined the uptake coefficients of H_2O_2 on $\text{PM}_{2.5}$ over the RH range
 295 of 3% to 90%. Before this experiment, we compared the measured uptake
 296 coefficients of H_2O_2 on two $\text{PM}_{2.5}$ samples, one had been used to measure the uptake
 297 coefficient of PAA and the other had not been used for any measurements. The
 298 results show that the relative error between the above two experiments was 1.0–7.4%
 299 among different RH (3–90%). Therefore, there is no obvious difference between the
 300 uptake coefficients of H_2O_2 on used and unused $\text{PM}_{2.5}$ samples. Figure 5 shows the
 301 $\gamma_{\text{H}_2\text{O}_2}$ on $\text{PM}_{2.5}$ which had been used to measure γ_{PAA} , over 3–90% RH. The
 302 empirical equation of $\gamma_{\text{H}_2\text{O}_2}$ as a function of $a_{\text{H}_2\text{O}}$ can be expressed as Eq. (15) and the
 303 measured and modelled $\gamma_{\text{H}_2\text{O}_2}$ on $\text{PM}_{2.5}$ is shown in Fig. 4.

$$\gamma_{\text{H}_2\text{O}_2} = \frac{5.32 \times 10^{-4}}{1 - 0.82 \times a_{\text{H}_2\text{O}}^{0.13}} \quad (15)$$

304 The value of $\gamma_{\text{H}_2\text{O}_2}$, similar to γ_{PAA} , shows a positive correlation with RH. The
 305 average value of $\gamma_{\text{H}_2\text{O}_2}$ changes from $(1.12 \pm 0.20) \times 10^{-4}$ at 3% RH to $(2.70 \pm 0.37) \times 10^{-4}$
 306 at 90% RH. The positive RH dependence of $\gamma_{\text{H}_2\text{O}_2}$ has been reported by Pradhan et al.
 307 (2010b). They have measured $\gamma_{\text{H}_2\text{O}_2}$ on authentic mineral dust particles (i.e., Gobi
 308 dust particles and Saharan dust particles). Table 4 summarizes the literature result of
 309 $\gamma_{\text{H}_2\text{O}_2}$ and its RH dependence on different type of mineral dust in literature data.
 310 Apart from $\gamma_{\text{H}_2\text{O}_2}$ on authentic Gobi dust, authentic Saharan dust and aged particles,
 311 all $\gamma_{\text{H}_2\text{O}_2}$ values show a negative RH dependence.

312 Figure 6 shows the ratio of $\gamma_{\text{PAA}, 90\% \text{ RH}}$ to $\gamma_{\text{PAA}, 3\% \text{ RH}}$ ($R_{\gamma_{\text{PAA}}}$) and $\gamma_{\text{H}_2\text{O}_2, 90\% \text{ RH}}$ to

313 $\gamma_{\text{H}_2\text{O}_2, 3\% \text{ RH}}$ ($R_{\gamma_{\text{H}_2\text{O}_2}}$). Although the $R_{\gamma_{\text{PAA}}}$ values are more variable on haze days than
314 those on non-haze days, the average value of $R_{\gamma_{\text{PAA}}}$ shows no obvious difference at
315 different times and under different weather conditions, varying over the narrow
316 range of 4.4 ± 0.6 to 6.3 ± 2.7 . On average, $R_{\gamma_{\text{PAA}}}$ is 5.4 ± 1.9 . It is interesting to note
317 that $R_{\gamma_{\text{H}_2\text{O}_2}}$ is 2.4 ± 0.5 (see Fig. 6b), which is much lower than $R_{\gamma_{\text{PAA}}}$. Although $\gamma_{\text{H}_2\text{O}_2}$
318 has a positive RH dependence on $\text{PM}_{2.5}$ as well, H_2O_2 is less sensitive to RH
319 variance compared to PAA. For peroxide compounds, if a physical process,
320 especially the dissolution, dominates their uptake on $\text{PM}_{2.5}$, the $R_{\gamma_{\text{H}_2\text{O}_2}}$ should be
321 larger than $R_{\gamma_{\text{PAA}}}$, because the Henry's law constant of H_2O_2 is 100 times larger than
322 that of PAA (298 K) ($8.47 \times 10^2 \text{ M atm}^{-1}$ for PAA and $8.43 \times 10^4 \text{ M atm}^{-1}$ for H_2O_2)
323 (O'Sullivan et al., 1996). This expectation, however, is at odds with our experimental
324 results. Hence, we speculate that physical process is not the main pathway for the
325 uptake of peroxide compounds on $\text{PM}_{2.5}$. In addition, the values of γ_{PAA} and $\gamma_{\text{H}_2\text{O}_2}$ on
326 $\text{PM}_{2.5}$ were measured with increasing RH from 3% to 90% and then the
327 measurements were repeated by using the same sample with decreasing RH from 90
328 to 3%. Interestingly, we find that the γ_{PAA} and $\gamma_{\text{H}_2\text{O}_2}$ can be well repeated in these two
329 cases (see Fig. 3 and Fig. 5). The independence of γ_{PAA} and $\gamma_{\text{H}_2\text{O}_2}$ on reaction time
330 also indicates that $\text{PM}_{2.5}$ has a sustained reactivity for the uptake of peroxide
331 compounds at different RH, which falls into the category of reactive uptake as
332 suggested by Crowley et al. (2010). The detailed mechanism is described in Section
333 3.3.

334 The present study is the first investigation on the kinetics of the heterogeneous
335 reactions of PAA and H_2O_2 on $\text{PM}_{2.5}$ particles. Recent studies have already indicated
336 the importance of mineral dust for H_2O_2 uptake (Pradhan et al., 2010a; Pradhan et al.,
337 2010b; Wang et al., 2011; Zhao et al., 2011a; Zhao et al., 2011b; Romanias et al.,
338 2012; Zhou et al., 2012; Romanias et al., 2013; Zhao et al., 2013; El Zein et al.,
339 2014). For PAA, however, no data regarding its kinetics on mineral dust has been
340 available in the literature. Therefore, we investigated the heterogeneous reaction of
341 PAA on mineral dust as a comparison of that on $\text{PM}_{2.5}$.

342 3.2 Uptake of PAA and H₂O₂ on mineral dust

343 Mineral dust is an important component of atmospheric aerosols in Beijing, it
344 comprises 6.0% and 6.2% of PM_{2.5} on haze days and non-haze days, which is similar
345 to the reported values (7.1%–12.9%) (Sun et al., 2004; Yang et al., 2011; Zhang et al.,
346 2013). To determine whether the mineral dust dominates the uptake of PAA on PM_{2.5},
347 we measured the γ_{PAA} on two kinds of mineral dust particles, i.e., ADS and ATD
348 particles. The measured γ_{PAA} values are listed in Table 3. γ_{PAA} on low mass ADS
349 (ADS_l) increases from $(0.84 \pm 0.01) \times 10^{-4}$ at 3% RH to $(3.21 \pm 0.08) \times 10^{-4}$ at 90% RH
350 and γ_{PAA} on high mass ADS (ADS_h) increases from $(1.37 \pm 0.02) \times 10^{-4}$ at 3% RH to
351 $(2.62 \pm 0.01) \times 10^{-4}$ at 90% RH. On the surface of ATD, however, γ_{PAA} shows a
352 negative RH dependence, from $(2.42 \pm 0.02) \times 10^{-4}$ at 3% RH to $(1.17 \pm 0.03) \times 10^{-4}$ at
353 90% RH on low mass ATD (ATD_l) and decreasing from $(1.86 \pm 0.01) \times 10^{-4}$ at 3% RH
354 to $(0.91 \pm 0.04) \times 10^{-4}$ at 90% RH on high mass ATD (ATD_h). Table 3 also lists the
355 lower limit of γ_{PAA} on ADS and ATD, which are calculated by the BET surface area
356 of the particles. The lower limits of γ_{PAA} on ADS and ATD are on the order of
357 10^{-6} – 10^{-5} . The positive correlations between RH and γ_{PAA} on ADS are similar to that
358 on PM_{2.5}. Similar positive RH dependence has also been observed for the uptake of
359 H₂O₂ on authentic Gobi dust, Saharan dust (Pradhan et al., 2010b) and aged CaCO₃
360 particles (Zhao et al., 2013). This negative RH dependence on ATD is similar to the
361 previously reported $\gamma_{\text{H}_2\text{O}_2}$ on ATD and mineral oxides (e.g., α -Al₂O₃, Fe₂O₃, TiO₂,
362 SiO₂) (Pradhan et al., 2010a; Zhao et al., 2011a; Romanias et al., 2012, 2013; El Zein
363 et al., 2014). The reasons for the discrepancies in the RH dependence of γ_{PAA} are
364 discussed in Sect. 3.3. The empirical equation of γ_{PAA} against $a_{\text{H}_2\text{O}}$ on ADS and ATD
365 can be expressed as Eq. (16) and (17), respectively:

$$\gamma_{\text{PAA}} = \frac{7.49 \times 10^{-5}}{1 - 0.76 \times a_{\text{H}_2\text{O}}^{0.25}} \quad (16)$$

$$\gamma_{\text{PAA}} = \frac{2.18 \times 10^{-4}}{1 + 1.08 \times a_{\text{H}_2\text{O}}^{1.06}} \quad (17)$$

366 We also determined the uptake coefficient of H_2O_2 on ADS and ATD over the RH
 367 range of 3 to 90%. The measured $\gamma_{\text{H}_2\text{O}_2}$ on ADS and ATD is shown in Fig. 7. The
 368 value of $\gamma_{\text{H}_2\text{O}_2}$, similar to γ_{PAA} , shows a positive correlation with RH on ADS
 369 particles and a negative correlation with RH on ATD particles. By taking the average
 370 of γ values at low and high mass loading, $\gamma_{\text{H}_2\text{O}_2}$ on ADS increases from
 371 $(1.10 \pm 0.31) \times 10^{-4}$ at 3% RH to $(2.44 \pm 0.69) \times 10^{-4}$ at 90% RH and the $\gamma_{\text{H}_2\text{O}_2}$ on ATD
 372 decreases from $(3.11 \pm 0.34) \times 10^{-4}$ at 3% RH to $(0.87 \pm 0.06) \times 10^{-4}$ at 90% RH.
 373 Although the values of $\gamma_{\text{H}_2\text{O}_2}$ at low and high mass loading are not identical, all $\gamma_{\text{H}_2\text{O}_2}$
 374 values on ADS show a positive correlation with RH, and all $\gamma_{\text{H}_2\text{O}_2}$ values on ATD
 375 show a negative correlation with RH. A_{es} for ADS_l and ADS_h is 6.1 cm^2 and 10.9
 376 cm^2 , respectively; A_{es} for ATD_l and ATD_h is 6.4 cm^2 and 11.2 cm^2 , respectively.

377 The empirical equation of γ_{PAA} against $a_{\text{H}_2\text{O}}$ on ADS and ATD can be expressed as
 378 Eq. (18) and (19), respectively:

$$\gamma_{\text{H}_2\text{O}_2} = \frac{9.97 \times 10^{-5}}{1 - 0.63 \times a_{\text{H}_2\text{O}}^{0.59}} \quad (18)$$

$$\gamma_{\text{H}_2\text{O}_2} = \frac{3.33 \times 10^{-4}}{1 + 3.02 \times a_{\text{H}_2\text{O}}^{1.07}} \quad (19)$$

379 It is noted that although the γ values of H_2O_2 and PAA on mineral dust particles
 380 obtained with the low mass loading are not the same with those with high mass
 381 loading, they have the same RH dependence. The difference among ADS_l , ADS_h ,
 382 ATD_l and ATD_h are mainly caused by two reasons: the uncertainty of the A_{es}
 383 estimation method and the experimental error.

384 3.3 Reaction mechanisms

385 In general, the uptake of a gas onto particles can be attributed to physical processes

386 (e.g., physisorption and dissolution) and/or chemical processes (e.g., catalytic
387 reaction, acid-base reaction, redox reaction and thermal decomposition). In Section
388 3.1, we have provided evidence that the chemical processes dominate the uptake of
389 peroxide compounds on PM_{2.5}. Here, we discuss the potential chemical pathways.

390 The composition of PM_{2.5} determines the relative importance of physical and
391 chemical processes. In general, PM_{2.5} is mainly composed of mineral dust, sulfate,
392 nitrate, ammonium compounds, soot, and organic matter (Eldred et al., 1997; He et
393 al., 2001; Hueglin et al., 2005; Sun et al., 2006; Huang et al., 2014). In this study, we
394 have measured the concentrations of elements and soluble ions in PM_{2.5} samples.
395 The results are shown in Table 5. The concentration of mineral dust was estimated
396 by multiplying 14.3 by the concentration of Al element, the ratio was suggested by
397 Zhang et al. (2013) for PM_{2.5} in urban Beijing. The estimated mineral dust accounts
398 for 6.0±4.3% and 6.2±3.1% of PM_{2.5} mass concentration on haze days and non-haze
399 days, respectively. The concentration of SO₄²⁻ is 42.26±7.88 μg m⁻³ on haze days,
400 which is about seven times of that on non-haze days. The concentration of NO₃⁻ and
401 Cl⁻ on haze days are also about 6.9–7.3 times of those on non-haze days.

402 There have been several studies of the mechanism of H₂O₂ uptake on mineral dust
403 particles. Zhao et al. (2011a) have found that the uptake of H₂O₂ on both SiO₂ and
404 α-Al₂O₃ particles decreased with increasing RH. On SiO₂ particles, the contribution
405 of physisorption to H₂O₂ uptake increased from 59% at 12% RH to 80% at 76% RH;
406 on α-Al₂O₃ particles, the catalytic decomposition dominated H₂O₂ uptake even at
407 high RH probably due to its high surface reactivity. Although the γ_{H₂O₂} on both SiO₂
408 and α-Al₂O₃ particles decreased with increasing RH, the reduction was more
409 pronounced on the physical process dominated SiO₂ particles. El Zein et al. (2014)
410 observed a negative correlation between RH and γ_{H₂O₂} on ATD particles and
411 suggested that the uptake of H₂O₂ on ATD particles was a catalytic process and it
412 was not limited by site-filling. Thus, the catalytic reaction of mineral dust might be
413 important to the uptake of peroxide compounds on PM_{2.5}. But this reaction alone
414 cannot explain the positive RH dependence for the γ on PM_{2.5}. Therefore, some other

415 pathways may also important to the uptake of peroxide compounds onto PM_{2.5}.
416 Based on the characteristics of peroxide compounds, in addition to catalytic reaction,
417 acid-base reaction, redox reaction, thermal decomposition, and aqueous reaction are
418 considered as the potential pathways.

419 With respect to acid-base reactions, we must consider that H₂O₂ and PAA are both
420 weak acids (pK_a=11.6 for H₂O₂, Marinoni et al., 2011; pK_a=8.2 for PAA, Evans and
421 Upton, 1985) and can react with alkaline substances. A number of studies have
422 demonstrated that the heterogeneous reaction of an acidic vapor on alkaline materials
423 is enhanced with increasing RH (Santschi and Rossi, 2006; Preszler et al., 2007;
424 Sullivan et al., 2009). However, PM_{2.5} in Beijing is acidic (e.g., pH=5.57, Wang et al.,
425 2005). The concentrations of ions of strong acids such as SO₄²⁻ and NO₃⁻ make up
426 60.9% of PM_{2.5} mass on haze days, and 41.3% on non-haze days (see Table 5). Even
427 though there are some basic components (such as NH₄⁺ and CaCO₃), we believe they
428 are already neutralized or acidified. Therefore, acid-base reactions on PM_{2.5} may not
429 be important for the uptake of H₂O₂ and PAA.

430 Both PAA and H₂O₂ have strong oxidative capacity and can react with the
431 reducing substances on aerosol particles, especially in the presence of water. Zhao et
432 al. (2013) found that $\gamma_{\text{H}_2\text{O}_2}$ on sulfite-coated calcium carbonate particles is 3–10
433 times higher than that on the pristine calcium carbonate particles. This enhancement
434 increased with increasing RH. In addition, transition metals make up 0.9% of PM_{2.5}
435 mass on haze days and 1.2% on non-haze days. Both PAA and H₂O₂ can undergo
436 catalytic reactions with transition metals, leading to the formation of highly reactive
437 species, such as OH, RO and RO₂ radicals (Koubek and Edwards, 1963; Lin and
438 Gurol, 1998; Zhang et al., 1998; Hiroki and LaVerne, 2005). Nawrot et al., (2009)
439 have studied PM_{2.5} samples in 20 European locations and suggested that H₂O₂ would
440 decompose and form OH radicals in the presence of transition metals (i.e. Cu, Fe,
441 Mn, Pb, V and Ti). Petigara et al. (2002) have reported that the decomposition rate of
442 H₂O₂ is enhanced by the presence of organic matter and manganese. Therefore, the
443 redox reactions may be important to the uptake of peroxide compounds on PM_{2.5}.

444 It is noted that PAA, which has a hydroperoxyl group (–OOH) and a carbonyl
445 group (C=O), is less stable than H₂O₂ (Kunigk et al., 2012) and can more readily
446 undergo thermal decomposition. The O–O bond dissociation enthalpies at 298 K of
447 PAA and H₂O₂ are 48 kcal mol^{–1} and 50 kcal mol^{–1}, respectively (Bach et al., 1996).
448 In addition, PAA is prone to hydrolysis in the presence of water (Reaction 3 and
449 Reaction 4) (Yuan et al., 1997). This is consistent with our experimental result that
450 $R_{\gamma\text{PAA}}$ is larger than $R_{\gamma\text{H}_2\text{O}_2}$.



451 In considering the role of aqueous reactions, water soluble inorganic salts
452 including sulfate and nitrate make up a substantial fraction (35–58%) of PM_{2.5} (Sun
453 et al., 2004; Wang et al., 2005). As shown in Table 5, the concentration of Cl[–], NO₃[–]
454 and SO₄^{2–} accounts for 61.9% and 42.0% of PM_{2.5} mass on haze days and non-haze
455 days, respectively. These salts can greatly increase the water content of the particles
456 under humid conditions. When RH exceeds the deliquescence relative humidity
457 (DRH) of these inorganic salts, PM_{2.5} may be covered with an aqueous film on the
458 particle surface or exist in a liquid phase state. The DRH is suggested to be 79% for
459 (NH₄)₂SO₄, 39% for NH₄HSO₄ and 62% for NH₄NO₃ at 298K (Cziczo et al., 1997;
460 Lightstone et al., 2000), and the DRH of PM_{2.5} is even lower than that of the
461 individual salt particles (Seinfeld and Pandis, 2006). Under humid conditions, the
462 deliquesced particles and/or the aqueous film on the particle surface becomes a
463 medium for aqueous reaction. In this aqueous phase, soluble salts will release anions.
464 The anions can potentially enhance the dissolution of Fe minerals (Rubasinghege et
465 al., 2010), resulting in a larger uptake of peroxide compounds by Fe catalysis
466 (Chevallier et al., 2004; Pignatello et al., 2006). Furthermore, Zhao et al. (2013) have
467 provided experimental evidence for the effect of a soluble salt on $\gamma_{\text{H}_2\text{O}_2}$. They found
468 that nitrate coated on calcium carbonate particles decreased the $\gamma_{\text{H}_2\text{O}_2}$ by 30–85% at
469 3% RH, but increases $\gamma_{\text{H}_2\text{O}_2}$ by a factor of 1–8 with increasing RH from 20 to 75%,

470 as compared to the $\gamma_{\text{H}_2\text{O}_2}$ on the uncoated particles. Mineral dust can undergo
471 atmospheric aging from its emission, which modifies its surface with coating sulfates
472 and nitrates (Sullivan et al., 2007). The aged authentic mineral dust particles (e.g.,
473 ADS dust, Gobi dust and Saharan dust) are coated with salts, while the mineral oxide
474 (e.g., SiO_2 , TiO_2 and $\alpha\text{-Al}_2\text{O}_3$) and ATD particles have no or few soluble salts
475 coating. For example, in this study, the measured concentration of SO_4^{2-} in ADS and
476 ATD particles was $20.3 \mu\text{g mg}^{-1}$ and $0.2 \mu\text{g mg}^{-1}$, respectively. The coatings on the
477 particles can lead to the formation of a surface aqueous film, in which the aqueous
478 reactions may occur. This observation helps explain the differences in RH
479 dependence of the uptake of peroxides on aged authentic particles and unaged
480 mineral oxide and ATD particles. In short, the aqueous reactions that occur in the
481 aqueous film or liquid particles formed by the deliquescence of soluble salts may
482 play important roles in the uptake of peroxide compounds on $\text{PM}_{2.5}$ and aged mineral
483 dust particles.

484 In summary, chemical processes rather than physical processes dominate the
485 heterogeneous reaction of peroxide compounds on $\text{PM}_{2.5}$ and aged mineral dust
486 particles. The inorganic soluble components in authentic particles play an important
487 role in the uptake of peroxide compounds. The uptake of peroxide compounds on
488 $\text{PM}_{2.5}$ is probably affected by the combined effects of catalytic reactions, redox
489 reactions, thermal decomposition, and aqueous reactions.

490 **4 Conclusions and Implications**

491 The present study is the first to measure the uptake coefficient of gaseous PAA and
492 H_2O_2 on ambient $\text{PM}_{2.5}$ and on mineral dust over a wide range of RH values (3–
493 90%). Both of γ_{PAA} and $\gamma_{\text{H}_2\text{O}_2}$ on $\text{PM}_{2.5}$ have a positive correlation with RH. In
494 general, both γ_{PAA} and $\gamma_{\text{H}_2\text{O}_2}$ are on the order of 10^{-4} . The γ_{PAA} values show no
495 obvious differences between haze days and non-haze days. Both γ_{PAA} and $\gamma_{\text{H}_2\text{O}_2}$ on
496 Asian Dust Storm (ADS) particles shows a similar RH dependence compared to
497 $\text{PM}_{2.5}$, but on Arizona Test Dust (ATD), both γ_{PAA} and $\gamma_{\text{H}_2\text{O}_2}$ show a negative RH
498 dependence. This observation provides evidence that in addition to the mineral dust,

499 other components in PM_{2.5}, such as soluble inorganic salts and organic compounds
500 may greatly contribute to the uptake of peroxide compounds. The ratio of $\gamma_{\text{PAA}, 90\% \text{ RH}}$
501 to $\gamma_{\text{PAA}, 3\% \text{ RH}}$ ($R_{\gamma_{\text{PAA}}}$) is larger than the ratio of $\gamma_{\text{H}_2\text{O}_2, 90\% \text{ RH}}$ to $\gamma_{\text{H}_2\text{O}_2, 3\% \text{ RH}}$ ($R_{\gamma_{\text{H}_2\text{O}_2}}$),
502 while the Henry's law constant of H₂O₂ is 100 times that of PAA; besides, authentic
503 particles show a sustained surface reactivity for the uptake of peroxide compounds.
504 These two experimental results suggest that chemical processes dominate the uptake
505 of peroxide compounds onto PM_{2.5} and aged mineral dust. The potential chemical
506 processes include catalytic reactions, redox reactions, thermal decomposition and
507 aqueous reactions. The heterogeneous processes of H₂O₂ have already been taken
508 into account as an important removal pathway (de Reus et al., 2005; Liang et al.,
509 2013). To the best of our knowledge, there has been almost no consideration of the
510 heterogeneous removal pathways for organic peroxides.

511 Field observations have shown that the atmospheric lifetime of PAA is 4.1–5.8 h
512 in summer in Beijing (Zhang et al., 2010; Liang et al., 2013). To explain this result,
513 we at first considered the traditional removal mechanism for PAA, including the gas
514 phase chemical reactions (OH radical reaction and photolysis) and deposition
515 (Jackson and Hewitt, 1999). The concentration of OH radicals has a positive
516 correlation with solar ultraviolet irradiation and changes in different seasons. The
517 mean concentration of OH radicals on non-haze summer day was estimated as
518 3.4×10^6 molecule cm⁻³ in the 35–45 °N area (Bahm and Khalil, 2004), where Beijing
519 is located. In addition, the concentration of OH radicals on a haze day is one fourth
520 of that on a non-haze day (Liang et al., 2013). The reaction rate constant of OH
521 radical with PAA is 3.7×10^{-12} cm³ molecule⁻¹ s⁻¹ (Jenkin et al., 1997; Saunders et al.,
522 2003). Hence, the lifetime of PAA with respect to the OH radical reaction is 88.3 h
523 on a haze day and 22.1 h on a non-haze day. Using the reported cross sections of
524 PAA by Orlando and Tyndall (2003), the lifetime of PAA against photolysis is about
525 28 d on haze days and 21 d on non-haze days. In these studies, we assume that the
526 planetary boundary layer is 1000 m and the dry deposition of PAA is 0.27 cm s⁻¹
527 (Wesely, 1989; Hall et al., 1999), both on haze and non-haze days. The lifetime of

528 PAA against dry deposition is 4.3 d. The estimated overall lifetime of PAA is 44.2 h
 529 on a haze day and 17.6 h on a non-haze day. Obviously, this lifetime is much longer
 530 than the field observation results, especially on haze days, indicating that the
 531 heterogeneous reaction of PAA on ambient particles would be a removal pathway for
 532 gaseous PAA.

533 In order to estimate the PAA lifetime with respect to the heterogeneous reactions,
 534 we assume that all PM_{2.5} particles are spheres and the heterogeneous reaction of PAA
 535 on PM_{2.5} is a pseudo-first-order reaction. The lifetime of PAA can be calculated by
 536 Eq. (20) (Ravishankara, 1997):

$$\tau = \frac{[C]}{d[C]/dt} = \frac{4}{\gamma \omega A_v} \quad (20)$$

537 where A_v is the surface area per unit volume of PM_{2.5}, m² m⁻³. Assuming each mode
 538 of aerosol fine particles is a log-normal distribution, the particles number can be
 539 expressed as Eq. (21) (Seinfeld and Pandis, 2006):

$$\frac{dN}{d\log D_p} = \sum_i^n \frac{N_i}{\sqrt{2\pi} \log \sigma_i} \exp\left(-\frac{(\log D_p - \log \overline{D_{p_i}})^2}{2 \log^2 \sigma_i}\right) \quad (21)$$

540 where $i = 1, 2, 3$ corresponding to the nucleation mode (3–20 nm), Aiken mode (20–
 541 100 nm), and accumulation mode (100–1000 nm), respectively; N_i is the number
 542 concentration; $\overline{D_{p_i}}$ is the geometric mean diameter, m; σ_i is the geometric standard
 543 deviation of the i th mode. The recommended values of $N_{i,i}$, $\overline{D_{p_i}}$ and σ_i are suggested
 544 by Yue et al. (2009). The value of A_v can be calculated by Eq. (22):

$$A_v = \frac{6M_a}{\rho \overline{D_p} V} \quad (22)$$

545 where M_a is the mass of the PM_{2.5} particles, kg; ρ is the density of the PM_{2.5} particles,
 546 1.42×10^3 kg m⁻³ for a haze period and 1.96×10^3 kg m⁻³ for a non-haze period (Hu et
 547 al., 2012); $\overline{D_p}$ is the mean diameter of the total particles, m; V is the volume of
 548 sampling air, m³. The number percentage of coarse mode particles (1000–2500 nm)

549 is less than 0.02% of the fine particles number (3–1000 nm) (Wu et al., 2008) and
550 the corresponding surface area of the coarse mode is about 0.4% of the total surface
551 area. Therefore, the surface area of the coarse mode particles (1000–2500 nm) could
552 be negligible and \overline{Dp} is 114.6 nm for haze days PM_{2.5} particles and 62.4 nm for
553 non-haze PM_{2.5} particles. The mean mass concentration is 123 $\mu\text{g m}^{-3}$ on a haze day
554 and 23 $\mu\text{g m}^{-3}$ on a non-haze day and the corresponding A_v is $4.5 \times 10^3 \mu\text{m}^2 \text{cm}^{-3}$ on a
555 haze day and $1.2 \times 10^3 \mu\text{m}^2 \text{cm}^{-3}$ on a non-haze day, which is similar to the literature
556 results (Wehner et al., 2008; He et al., 2010). Here, we use the mean uptake
557 coefficient of PAA on PM_{2.5} at 60% RH, i.e., $\gamma = 2.70 \times 10^{-4}$, to estimate the lifetime of
558 PAA. The calculated lifetime of PAA against heterogeneous reaction is 3.2 h on a
559 haze day and 11.9 h on a non-haze day, which are more important than photolysis
560 and decomposition and can compete with OH reaction on haze days. Considering
561 heterogeneous reaction, gas phase reaction and deposition, the estimated lifetime of
562 PAA is 3.0 h on a haze day and 7.1 h on a non-haze day, which is similar to the field
563 measurement results. Thus, the heterogeneous reaction on PM_{2.5} is likely to be an
564 important removal pathway for PAA.

565 The fate of peroxide compounds on aerosols will greatly impact the budget of
566 peroxide compounds themselves as well as the cycle of radicals in the atmosphere.
567 The formation of PAA and H₂O₂ is related to the self-reaction of HO₂ radical and the
568 reaction of HO₂ radical with RO₂ radical, while the photolysis of PAA and H₂O₂
569 release HO_x radical and RO_x radical. Therefore, peroxide compounds can be treated
570 as a temporary reservoir of HO_x radicals and RO_x radicals. Besides, PAA has a close
571 relation with peroxyacetyl nitrate (PAN). In high NO_x (NO+NO₂) areas, such as
572 urban areas, NO₂ will combine with acetyl peroxy (CH₃C(O)OO) radical to form
573 PAN by competing with HO₂ radical which will donate H to the CH₃C(O)OO radical
574 to form PAA. The uptake of PAA onto the particle surface will result in a sink for the
575 CH₃C(O)OO radical, hence reducing PAN, which is an important carrier of NO_x and
576 regionally transports NO_x from urban areas to rural and remote areas, affecting
577 oxidant (e.g., O₃ and OH radical) distribution there (Fischer et al., 2014). Moreover,

578 through the heterogeneous uptake, the peroxide compounds are introduced onto the
579 surface of particles, which might enhance the atmospheric aerosol oxidative capacity
580 and then change the composition of the aerosols. For example, Zhao et al. (2014)
581 have suggested that the coexistence of H₂O₂ could enhance heterogeneous oxidation
582 of OVOCs and the yield of organic acids, such as formic acid and acetic acid.
583 Moreover, peroxide compounds, have the potential to enhance the heterogeneous
584 reaction of SO₂ and promote sulfate formation. Hence, the heterogeneous reaction of
585 peroxide compounds on aerosols may help to explain the high concentration of
586 sulfates during haze episodes when other oxidants (e.g., OH radicals) are limited.
587 Therefore, we suggest that the current atmospheric models should take into account
588 the heterogeneous reactions of peroxide compounds on aerosols.

589 *Acknowledgements.* We gratefully acknowledge the National Natural Science
590 Foundation of China (grants 41275125, 21190053, 21477002) and the State Key
591 Laboratory of Environment Simulation and Pollution Control (special fund) for
592 financial support. We thank Professor L. M. Zeng (Peking University) for providing
593 TH-16A PM_{2.5} sampler.

594 **References**

- 595 Atkinson, R., Aschmann, S. M., Arey, J., and Shorees, B.: Formation of OH radicals
596 in the gas phase reactions of O₃ with a series of terpenes, *J. Geophys. Res.*, 97,
597 6065–6073, doi: 10.1029/92jd00062, 1992.
- 598 Bach, R. D., Ayala, P. Y., and Schlegel, H. B.: A reassessment of the bond
599 dissociation energies of peroxides. An ab Initio Study, *J. Am. Chem. Soc.*, 118,
600 12758–12765, doi:10.1021/ja961838i, 1996.
- 601 Bahm, K. and Khalil, M. A. K.: A new model of tropospheric hydroxyl radical
602 concentrations, *Chemosphere*, 54, 143–166, doi:
603 10.1016/j.chemosphere.2003.08.006, 2004.
- 604 Bedjanian, Y., Romanias, M. N., and El Zein, A.: Uptake of HO₂ radicals on Arizona
605 Test Dust, *Atmos. Chem. Phys.*, 13, 6461–6471, doi: 10.5194/acp-13-6461-2013,
606 2013.

607 Calvert, J. G., Lazrus, A., Kok, G. L., Heikes, B. G., Walega, J. G., Lind, J., and
608 Cantrell, C. A.: Chemical mechanisms of acid generation in the troposphere,
609 Nature, 317, 27–35, doi: 10.1038/317027a0, 1985.

610 Chevallier, E., Jolibois, R. D., Meunier, N., Carlier, P., and Monod, A.: “Fenton-like”
611 reactions of methylhydroperoxide and ethylhydroperoxide with Fe²⁺ in liquid
612 aerosols under tropospheric conditions, Atmos. Environ., 38, 921–933, doi:
613 10.1016/j.atmosenv.2003.10.027, 2004.

614 Claeys, M., Wang, W., Ion, A. C., Kourtchev, I., Gelencsér, A., and Maenhaut, W.:
615 Formation of secondary organic aerosols from isoprene and its gas-phase
616 oxidation products through reaction with hydrogen peroxide, Atmos. Environ., 38,
617 4093–4098, doi: 10.1016/j.atmosenv.2004.06.001, 2004.

618 Crowley, J. N., Ammann, M., Cox, R. A., Hynes, R. G., Jenkin, M. E., Mellouki, A.,
619 Rossi, M. J., Troe, J., and Wallington, T. J.: Evaluated kinetic and photochemical
620 data for atmospheric chemistry: Volume V – heterogeneous reactions on solid
621 substrates, Atmos. Chem. Phys., 10, 9059–9223, doi: 10.5194/acp-10-9059-2010,
622 2010.

623 Cziczo, D. J., Nowak, J. B., Hu, J. H., and Abbatt, J. P. D.: Infrared spectroscopy of
624 model tropospheric aerosols as a function of relative humidity: Observation of
625 deliquescence and crystallization, J. Geophys. Res., 102, 18843–18850, doi:
626 10.1029/97jd01361, 1997.

627 de Reus, M., Fischer, H., Sander, R., Gros, V., Kormann, R., Salisbury, G., Van
628 Dingenen, R., Williams, J., Zöllner, M., and Lelieveld, J.: Observations and model
629 calculations of trace gas scavenging in a dense Saharan dust plume during
630 MINATROC, Atmos. Chem. Phys., 5, 1787–1803, doi: 10.5194/acp-5-1787-2005,
631 2005.

632 Docherty, K. S., Wu, W., Lim, Y. B., and Ziemann, P. J.: Contributions of organic
633 peroxides to secondary aerosol formed from reactions of monoterpenes with O₃,
634 Environ. Sci. Technol., 39, 4049–4059, doi: 10.1021/es050228s, 2005.

635 Dul’neva, L. V., and Moskvina, A. V.: Kinetics of formation of peroxyacetic acid,
636 Russ. J. Gen. Chem., 75, 1125–1130, doi: 10.1007/s11176-005-0378-8, 2005.

637 El Zein, A., Romanias, M. N., and Bedjanian, Y.: Heterogeneous interaction of H₂O₂
638 with Arizona Test Dust, *J. Phys. Chem. A*, 118, 441–448, doi: 10.1021/jp409946j,
639 2014.

640 Eldred, R. A., Cahill, T. A., and Flocchini, R. G.: Composition of PM_{2.5} and PM₁₀
641 aerosols in the IMPROVE Network, *J. Air Waste Manage.*, 47, 194–203,
642 10.1080/10473289.1997.10464422, 1997.

643 Evans, D. F. and Upton, M. W.: Studies on singlet oxygen in aqueous solution. Part 3.
644 The decomposition of peroxy-acids, *J. Chem. Soc., Dalton Transactions*, 1151–
645 1153, doi: 10.1039/dt9850001151, 1985.

646 Fischer, E. V., Jacob, D. J., Yantosca, R. M., Sulprizio, M. P., Millet, D. B., Mao, J.,
647 Paulot, F., Singh, H. B., Roiger, A., Ries, L., Talbot, R. W., Dzepina, K., and
648 Pandey Deolal, S.: Atmospheric peroxyacetyl nitrate (PAN): Aglobal budget and
649 source attribution, *Atmos. Chem. Phys.*, 14, 2679–2698, doi:
650 10.5194/acp-14-2679-2014, 2014.

651 Hall, B., Claiborn, C., and Baldocchi, D.: Measurement and modeling of the dry
652 deposition of peroxides, *Atmos. Environ.*, 33, 577–589, doi:
653 10.1016/s1352-2310(98)00271-4, 1999.

654 He, K., Yang, F., Ma, Y., Zhang, Q., Yao, X., Chan, C. K., Cadle, S., Chan, T., and
655 Mulawa, P.: The characteristics of PM_{2.5} in Beijing, China, *Atmos. Environ.*, 35,
656 4959–4970, doi: 10.1016/s1352-2310(01)00301-6, 2001.

657 He, S. Z., Chen, Z. M., Zhang, X., Zhao, Y., Huang, D. M., Zhao, J. N., Zhu, T., Hu,
658 M., and Zeng, L. M.: Measurement of atmospheric hydrogen peroxide and organic
659 peroxides in Beijing before and during the 2008 Olympic Games: Chemical and
660 physical factors influencing their concentrations, *J. Geophys. Res.*, 115, D17307,
661 doi: 10.1029/2009jd013544, 2010.

662 Hiroki, A. and LaVerne, J. A.: Decomposition of hydrogen peroxide at water-ceramic
663 oxide interfaces, *J. Phys. Chem. B*, 109, 3364–3370, doi: 10.1021/jp046405d,
664 2005.

665 Hu, M., Peng, J., Sun, K., Yue, D., Guo, S., Wiedensohler, A., and Wu, Z.:
666 Estimation of size-Resolved ambient particle density based on the measurement of

667 aerosol number, mass, and chemical size distributions in the winter in Beijing,
668 *Environ. Sci. Technol.*, 46, 9941–9947, doi: 10.1021/es204073t, 2012.

669 Hua, W., Chen, Z. M., Jie, C. Y., Kondo, Y., Hofzumahaus, A., Takegawa, N., Lu, K.
670 D., Miyazaki, Y., Kita, K., Wang, H. L., Zhang, Y. H., and Hu, M.: Atmospheric
671 hydrogen peroxide and organic hydroperoxides during PRIDE–PRD'06, China:
672 their concentration, formation mechanism and contribution to secondary aerosols,
673 *Atmos. Chem. Phys.*, 8, 10481–10530, doi: 10.5194/acp-8-6755-2008, 2008.

674 Huang, D., Chen, Z. M., Zhao, Y., and Liang, H.: Newly observed peroxides and the
675 water effect on the formation and removal of hydroxyalkyl hydroperoxides in the
676 ozonolysis of isoprene, *Atmos. Chem. Phys.*, 13, 5671–5683, doi:
677 10.5194/acp-13-5671-2013, 2013.

678 Huang, X. H. H., Bian, Q. J., Ng, W. M., Louie, P. K. K., and Yu, J. Z.:
679 Characterization of PM_{2.5} major components and source investigation in suburban
680 Hong Kong: A one year monitoring study, *Aerosol Air Qual. Res.*, 14, 237–250,
681 doi: 10.4209/aaqr.2013.01.0020, 2014.

682 Hueglin, C., Gehrig, R., Baltensperger, U., Gysel, M., Monn, C., and Vonmont, H.:
683 Chemical characterisation of PM_{2.5}, PM₁₀ and coarse particles at urban, near-city
684 and rural sites in Switzerland, *Atmos. Environ.*, 39, 637–651, doi:
685 10.1016/j.atmosenv.2004.10.027, 2005.

686 Jackson, A. V., and Hewitt, C. N.: Atmosphere hydrogen peroxide and organic
687 hydroperoxides: a review, *Crit. Rev. Environ. Sci. Technol.*, 29, 175–228, doi:
688 10.1080/10643389991259209, 1999.

689 Jenkin, M. E., Saunders, S. M., and Pilling, M. J.: The tropospheric degradation of
690 volatile organic compounds: a protocol for mechanism development, *Atmos.*
691 *Environ.*, 31, 81–104, doi: 10.1016/s1352-2310(96)00105-7, 1997.

692 Koubek, E. and Edwards, J. O.: The formation of cobaltic acetate in the catalytic
693 decomposition of peroxyacetic acid, *J. Inorg. Nucl. Chem.*, 25, 1401–1408, doi:
694 10.1016/0022-1902(63)80411-x, 1963.

695 Kunigk, L., Silva, S. M., and Jurkiewicz, C. H.: The Influence of temperature and
696 organic matter on the decomposition kinetics of peracetic acid in aqueous

697 solutions, *Lat. Am. Appl. Res.*, 42, 291–297,
698 doi:10.1590/S0104-66322001000200009, 2012.

699 Lee, M. H., Heikes, B. G., and O'Sullivan, D. W.: Hydrogen peroxide and organic
700 hydroperoxide in the troposphere: a review, *Atmos. Environ.*, 34, 3475–3494, doi:
701 10.1016/s1352-2310(99)00432-x, 2000.

702 Lee, M., Noone, B. C., O'sullivan, D., and Heikes, B. G.: Method for the collection
703 and HPLC analysis of hydrogenperoxide and C₁ and C₂ hydroperoxides in the
704 atmosphere, *J. Atmos. Ocean. Tech.*, 12, 1060–1070, doi:
705 10.1175/1520-0426(1995)012<1060:mftcah>2.0.co;2, 1995.

706 Li, W.: *Fundamentals of Aerosol Pollution Chemistry*, Yellow River Conservancy
707 Press, Zheng Zhou, 2010.

708 Liang, H., Chen, Z. M., Huang, D., Zhao, Y., and Li, Z. Y.: Impacts of aerosols on
709 the chemistry of atmospheric trace gases: A case study of peroxides and HO₂
710 radicals, *Atmos. Chem. Phys.*, 13, 11259–11276, doi: 10.5194/acp-13-11259-2013,
711 2013.

712 Lightfoot, P. D., Roussel, P., Caralp, F., and Lesclaux, R.: Flashphotolysis study of
713 the CH₃O₂ + CH₃O₂ and CH₃O₂ + HO₂ reactions between 600 and 719 K:
714 unimolecular decomposition of methylhydroperoxide, *J. Chem. Soc., Faraday T.*,
715 87, 3213–3220, doi: 10.1039/FT9918703213, 1991.

716 Lightstone, J. M., Onasch, T. B., Imre, D., and Oatis, S.: Deliquescence,
717 efflorescence, and water activity in ammonium nitrate and mixed ammonium
718 nitrate/succinic acid microparticles, *J. Phys. Chem. A*, 104, 9337–9346, doi:
719 10.1021/jp002137h, 2000.

720 Lin, S.S., and Gurol, M. D.: Catalytic decomposition of hydrogen peroxide on iron
721 oxide: Kinetics, mechanism, and implications, *Environ. Sci. Technol.*, 32, 1417–
722 1423, doi: 10.1021/es970648k, 1998.

723 Lind, J. A., Lazrus, A. L., and Kok, G. L.: Aqueous phase oxidation of sulfur(IV) by
724 hydrogen peroxide, methylhydroperoxide, and peroxyacetic acid, *J. Geophys. Res.*,
725 92, 4171–4177, doi: 10.1029/JD092iD04p04171, 1987.

726 Marinoni, A., Parazols, M., Brigante, M., Deguillaume, L., Amato, P., Delort, A.M.,

727 Laj, P., and Mailhot, G.: Hydrogen peroxide in natural cloud water: sources and
728 photoreactivity, *Atmos. Res.*, 101, 256–263, doi: 10.1016/j.atmosres.2011.02.013,
729 2011.

730 Molina, M. J., Molina, L. T., and Golden, D. M.: Environmental Chemistry (Gas and
731 Gas-Solid Interactions): The Role of Physical Chemistry, *J. Phys. Chem.*, 100,
732 12888–12896, doi: 10.1021/jp960146d, 1996

733 Nawrot, T. S., Kuenzli, N., Sunyer, J., Shi, T., Moreno, T., Viana, M., Heinrich, J.,
734 Forsberg, B., Kelly, F. J., Sughis, M., Nemery, B., and Borm, P.: Oxidative
735 properties of ambient PM_{2.5} and elemental composition: Heterogeneous
736 associations in 19 European cities, *Atmos. Environ.*, 43, 4595–4602, doi:
737 10.1016/j.atmosenv.2009.06.010, 2009.

738 Orlando, J. J. and Tyndall, G. S.: Gas phase UV absorption spectra for peracetic acid,
739 and for acetic acid monomers and dimers, *J. Photochem. Photobiol. A*, 157, 161–
740 166, doi: 10.1016/s1010-6030(03)00067-4, 2003.

741 O'Sullivan, D. W., Lee, M., Noone, B. C., and Heikes, B. G.: Henry's law constant
742 determinations for hydrogen peroxide, methyl hydroperoxide, hydroxymethyl
743 hydroperoxide, ethyl hydroperoxide, and peroxyacetic acid, *J. Phys. Chem.*, 100,
744 3241–3247, doi: 10.1021/jp951168n, 1996.

745 Paulot, F., Crounse, J. D., Kjaergaard, H. G., Kurten, A., St Clair, J. M., Seinfeld, J.
746 H., and Wennberg, P. O.: Unexpected epoxide formation in the gas-phase
747 photooxidation of isoprene, *Science*, 325, 730–733, doi: 10.1126/science.1172910,
748 2009.

749 Petigara, B. R., Blough, N. V., and Mignerey, A. C.: Mechanisms of hydrogen
750 peroxide decomposition in soils, *Environ. Sci. Technol.*, 36, 639–645, doi:
751 10.1021/es001726y, 2002.

752 Phillips, G. J., Pouvesle, N., Thieser, J., Schuster, G., Axinte, R., Fischer, H.,
753 Williams, J., Lelieveld, J., and Crowley, J. N.: Peroxyacetyl nitrate (PAN) and
754 peroxyacetic acid (PAA) measurements by iodide chemical ionisation mass
755 spectrometry: first analysis of results in the boreal forest and implications for the
756 measurement of PAN fluxes, *Atmos. Chem. Phys.*, 13, 1129–1139, doi:

757 10.5194/acp-13-1129-2013, 2013.

758 Pignatello, J. J., Oliveros, E., and MacKay, A.: Advanced oxidation processes for
759 organic contaminant destruction based on the Fenton reaction and related
760 chemistry, *Crit. Rev. Environ. Sci. Technol.*, 36, 1–84, doi:
761 10.1080/10643380500326564, 2006.

762 Pradhan, M., Kalberer, M., Griffiths, P. T., Braban, C. F., Pope, F. D., Cox, R. A., and
763 Lambert, R. M.: Uptake of gaseous hydrogen peroxide by submicrometer titanium
764 dioxide aerosol as a function of relative humidity, *Environ. Sci. Technol.*, 44,
765 1360–1365, doi: 10.1021/Es902916f, 2010a.

766 Pradhan, M., Kyriakou, G., Archibald, A. T., Papageorgiou, A. C., Kalberer, M., and
767 Lambert, R. M.: Heterogeneous uptake of gaseous hydrogen peroxide by Gobi and
768 Saharan dust aerosols: a potential missing sink for H₂O₂ in the troposphere, *Atmos.*
769 *Chem. Phys.*, 10, 7127–7136, doi: 10.5194/acp-10-7127-2010, 2010b.

770 Preszler P. A., Grassian, V. H., Kleiber, P., and Young, M. A.: Heterogeneous
771 conversion of calcite aerosol by nitric acid, *Phys. Chem. Chem. Phys.*, 9, 622–634,
772 doi: 10.1039/b613913b, 2007.

773 Ravetta, F., Jacob, D. J., Brune, W. H., Heikes, B. G., Anderson, B. E., Blake, D. R.,
774 Gregory, G. L., Sachse, G. W., Sandholm, S. T., Shetter, R. E., Singh, H. B., and
775 Talbot, R. W.: Experimental evidence for the importance of convected
776 methylhydroperoxide as a source of hydrogen oxide (HO_x) radicals in the tropical
777 upper troposphere, *J. Geophys. Res.*, 106, 32709–32716, doi:
778 10.1029/2001jd900009, 2001.

779 Ravishankara, A. R.: Heterogeneous and multiphase chemistry in the troposphere,
780 *Science*, 276, 1058–1065, doi: 10.1126/science.276.5315.1058, 1997.

781 Reeves, C. E., and Penkett, S. A.: Measurements of peroxides and what they tell us,
782 *Chem. Rev.*, 103, 5199–5218, doi: 10.1021/cr0205053, 2003.

783 Romanias, M. N., El Zein, A., and Bedjanian, Y.: Heterogeneous interaction of H₂O₂
784 with TiO₂ surface under dark and UV light irradiation conditions, *J. Phys. Chem.*
785 *A*, 116, 8191–8200, doi: 10.1021/jp305366v, 2012.

786 Romanias, M. N., El Zein, A., and Bedjanian, Y.: Uptake of hydrogen peroxide on

787 the surface of Al_2O_3 and Fe_2O_3 , *Atmos. Environ.*, 77, 1–8, doi:
788 10.1016/j.atmosenv.2013.04.065, 2013.

789 Rubasinghege, G., Lentz, R. W., Scherer, M. M., and Grassian, V. H.: Simulated
790 atmospheric processing of iron oxyhydroxide minerals at low pH: roles of particle
791 size and acid anion in iron dissolution, *Proc. Natl. Acad. Sci. USA*, 107, 6628–
792 6633, doi: 10.1073/pnas.0910809107, 2010.

793 Santschi, C., and Rossi, M. J.: Uptake of CO_2 , SO_2 , HNO_3 and HCl on calcite
794 (CaCO_3) at 300 K: mechanism and the role of adsorbed water, *J. Phys. Chem. A*,
795 110, 6789–6802, doi: 10.1021/jp056312b, 2006.

796 Saunders, S. M., Jenkin, M. E., Derwent, R. G., and Pilling, M. J.: Protocol for the
797 development of the Master Chemical Mechanism, MCM v3 (Part A):
798 Tropospheric degradation of non-aromatic volatile organic compounds, *Atmos.*
799 *Chem. Phys.*, 3, 161–180, doi: 10.5194/acp-3-161-2003, 2003.

800 Seinfeld, J. H., and Pandis, S. N.: *Atmospheric chemistry and physics: From air*
801 *pollution to climate change*, John Wiley & Sons, 2006.

802 Shen, X. L., Zhao, Y., Chen, Z. M., and Huang, D.: Heterogeneous reactions of
803 volatile organic compounds in the atmosphere, *Atmos. Environ.*, 68, 297–314,
804 doi:10.1016/j.atmosenv.2012.11.027,2013.

805 Stein, A. F. and Saylor, R. D.: Sensitivities of sulfate aerosol formation and oxidation
806 pathways on the chemical mechanism employed in simulations, *Atmos. Chem.*
807 *Phys.*, 12, 8567–8574, doi: 10.5194/acp-12-8567-2012, 2012.

808 Sullivan, R. C., Guazzotti, S. A., Sodeman, D. A., and Prather, K. A.: Direct
809 observations of the atmospheric processing of Asian mineral dust, *Atmos. Chem.*
810 *Phys.*, 7, 1213–1236, doi: 10.5194/acp-7-1213-2007, 2007.

811 Sullivan, R. C., Moore, M. J. K., Petters, M. D., Kreidenweis, S. M., Roberts, G. C.,
812 and Prather, K. A.: Timescale for hygroscopic conversion of calcite mineral
813 particles through heterogeneous reaction with nitric acid, *Phys. Chem. Chem.*
814 *Phys.*, 11, 7826–7837, doi: 10.1039/b904217b, 2009.

815 Sun, Y., Zhuang, G., Wang, Y., Han, L., Guo, J., Dan, M., Zhang, W., Wang, Z., and
816 Hao, Z.: The air-borne particulate pollution in Beijing – concentration,

817 composition, distribution and sources, *Atmos. Environ.*, 38, 5991–6004, doi:
818 10.1016/j.atmosenv.2004.07.009, 2004.

819 Sun, Y., Zhuang, G., Tang, A., Wang, Y., and An, Z.: Chemical characteristics of
820 PM_{2.5} and PM₁₀ in haze–fog episodes in Beijing, *Environ. Sci. Technol.*, 40,
821 3148–3155, doi: 10.1021/es051533g, 2006.

822 Surratt, J. D., Murphy, S. M., Kroll, J. H., Ng, N. L., Hildebrandt, L., Sorooshian, A.,
823 Szmigielski, R., Vermeylen, R., Maenhaut, W., Claeys, M., Flagan, R., and
824 Seinfeld, J. H.: Chemical composition of secondary organic aerosol formed from
825 the photooxidation of isoprene, *J. Phys. Chem. A.*, 110, 9665–9690, doi:
826 10.1021/jp061734m, 2006.

827 Vaghjiani, G. L. and Ravishankara, A. R.: Photodissociation of H₂O₂ and CH₃OOH
828 at 248 nm and 298 K: Quantum yields for OH, O(³P) and H(²S), *J. Chem. Phys.*,
829 92, 996–1003, doi: 10.1063/1.458081, 1990.

830 Wang, W. G., Ge, M. F., and Sun, Q.: Heterogeneous uptake of hydrogen peroxide
831 on mineral oxides, *Chinese J. Chem. Phys.*, 24, 515–520, doi:
832 10.1088/1674-0068/24/05/515-520, 2011.

833 Wang, Y., Zhuang, G., Tang, A., Yuan, H., Sun, Y., Chen, S., and Zheng, A.: The ion
834 chemistry and the source of PM_{2.5} aerosol in Beijing, *Atmos. Environ.*, 39, 3771–
835 3784, doi: 10.1016/j.atmosenv.2005.03.013, 2005.

836 Wallington, T. J., and Japar, S. M.: Reaction of CH₃O₂ + HO₂ in air at 295 K: a
837 product study, *Chem. Phys. Lett.*, 167, 513–518, doi:
838 10.1016/0009-2614(90)85461-K, 1990.

839 Wehner, B., Birmili, W., Ditas, F., Wu, Z., Hu, M., Liu, X., Mao, J., Sugimoto, N.,
840 and Wiedensohler, A.: Relationships between submicrometer particulate air
841 pollution and air mass history in Beijing, China, 2004–2006, *Atmos. Chem. Phys.*,
842 8, 6155–6168, doi: 10.5194/acp-8-6155-2008, 2008.

843 Wesely, M.: Parameterization of surface resistances to gaseous dry deposition in
844 regional-scale numerical models, *Atmos. Environ.*, 23, 1293–1304, doi:
845 10.1016/0004-6981(89)90153-4, 1989.

846 Wu, Z., Hu, M., Lin, P., Liu, S., Wehner, B., and Wiedensohler, A.: Particle number

847 size distribution in the urban atmosphere of Beijing, China, *Atmos. Environ.*, 42,
848 7967–7980, doi: 10.1016/j.atmosenv.2008.06.022, 2008.

849 Xu, L., Kollman, M. S., Song, C., Shilling, J. E., and Ng, N. L.: Effects of NO_x on
850 the volatility of secondary organic aerosol from isoprene photooxidation, *Environ.*
851 *Sci. Technol.*, 48, 2253–2262, doi: 10.1021/es404842g, 2014.

852 Yang, F., Tan, J., Zhao, Q., Du, Z., He, K., Ma, Y., Duan, F., Chen, G., and Zhao, Q.:
853 Characteristics of PM_{2.5} speciation in representative megacities and across China,
854 *Atmos. Chem. Phys.*, 11, 5207–5219, doi: 10.5194/acp-11-5207-2011, 2011.

855 Yuan, Z., Ni, Y., and Van Heiningen, A. R. P.: Kinetics of the peracetic acid
856 decomposition: Part II: pH effect and alkaline hydrolysis, *Can. J. Chem. Eng.*, 75,
857 42–47, doi: 10.1002/cjce.5450750109, 1997.

858 Yue, D., Hu, M., Wu, Z., Wang, Z., Guo, S., Wehner, B., Nowak, A., Achtert, P.,
859 Wiedensohler, A., Jung, J., Kim, Y. J., and Liu, S.: Characteristics of aerosol size
860 distributions and new particle formation in the summer in Beijing, *J. Geophys.*
861 *Res.*, 114, D00G12, doi: 10.1029/2008jd010894, 2009.

862 Zhang, R., Jing, J., Tao, J., Hsu, S. C., Wang, G., Cao, J., Lee, C. S. L., Zhu, L.,
863 Chen, Z., Zhao, Y., and Shen, Z.: Chemical characterization and source
864 apportionment of PM_{2.5} in Beijing: seasonal perspective, *Atmos. Chem. Phys.*, 13,
865 7053–7074, doi: 10.5194/acp-13-7053-2013, 2013.

866 Zhang, X., Chen, Z. M., He, S. Z., Hua, W., Zhao, Y., and Li, J. L.: Peroxyacetic acid
867 in urban and rural atmosphere: concentration, feedback on PAN–NO_x cycle and
868 implication on radical chemistry, *Atmos. Chem. Phys.*, 10, 737–748, doi:
869 10.5194/acp-10-737-2010, 2010.

870 Zhang, X. Z., Francis, R. C., Dutton, D. B., and Hill, R. T.: Decomposition of
871 peracetic acid catalyzed by cobalt(II) and vanadium(V), *Can. J. Chemistry*, 76,
872 1064–1069, doi: 10.1139/v98-103, 1998.

873 Zhao, X. B., Zhang, T., Zhou, Y. J., and Liu, D. H.: Preparation of peracetic acid
874 from hydrogen peroxide Part 1: Kinetics for peracetic acid synthesis and
875 hydrolysis, *J. Mol. Catal. A-Chem.*, 271, 246–252, doi:
876 10.1016/j.molcata.2007.03.012, 2007.

877 Zhao, Y., Chen, Z., and Zhao, J.: Heterogeneous reactions of methacrolein and
878 methyl vinyl ketone on α -Al₂O₃ particles, *Environ. Sci. Technol.*, 44, 2035–2041,
879 doi: 10.1021/es9037275, 2010.

880 Zhao, Y., Chen, Z., Shen, X., and Zhang, X.: Kinetics and mechanisms of
881 heterogeneous reaction of gaseous hydrogen peroxide on mineral oxide particles,
882 *Environ. Sci. Technol.*, 45, 3317–3324, doi: 10.1021/es104107c, 2011a.

883 Zhao, Y., Chen, Z. M., Shen, X. L., and Huang, D.: Importance of atmospheric aging
884 in reactivity of mineral dust aerosol: a case study of heterogeneous reaction of
885 gaseous hydrogen peroxide on processed mineral particles, *Atmos. Chem. and
886 Phys. Discuss.*, 11, 28563–28586, doi: 10.5194/acpd-11-28563-2011, 2011b.

887 Zhao, Y., Chen, Z., Shen, X., and Huang, D.: Heterogeneous reactions of gaseous
888 hydrogen peroxide on pristine and acidic gas-processed calcium carbonate
889 particles: Effects of relative humidity and surface coverage of coating, *Atmos.
890 Environ.*, 67, 63–72, doi: 10.1016/j.atmosenv.2012.10.055, 2013.

891 Zhao, Y., Huang, D., Huang, L., and Chen, Z.: Hydrogen peroxide enhances the
892 oxidation of oxygenated volatile organic compounds on mineral dust particles: a
893 case study of methacrolein, *Environ. Sci. Technol.*, 48, 10614–10623, doi:
894 10.1021/es5023416, 2014.

895 Zhao, Y., Wingen, L. M., Perraud, V., Greaves, J., and Finlayson-Pitts, B. J.: Role of
896 the reaction of stabilized Criegee intermediates with peroxy radicals in particle
897 formation and growth in air, *Phys. Chem. Chem. Phys.*, 17, 12500–12514, doi:
898 10.1039/c5cp01171j, 2015.

899 Zhou, L., Wang, W.G., and Ge, M.F.: Temperature dependence of heterogeneous
900 uptake of hydrogen peroxide on silicon dioxide and calcium carbonate, *J. Phys.
901 Chem. A*, 116, 7959–7964, doi: 10.1021/jp304446y, 2012.

902

Table 1. Comparison of γ_{PAA} on exposed and unexposed $\text{PM}_{2.5}$ filters (60% RH).

Sample	Exposed $\text{PM}_{2.5}$ particles	Unexposed $\text{PM}_{2.5}$ particles
Aug 01 ^a	2.08×10^{-4}	2.03×10^{-4}
Aug 01 ^b	2.29×10^{-4}	2.23×10^{-4}
Aug 05 ^a	2.30×10^{-4}	2.40×10^{-4}
Aug 05 ^b	2.45×10^{-4}	2.33×10^{-4}

Note: ^a daytime; ^b nighttime; exposed $\text{PM}_{2.5}$ particles, which has been used in the PAA uptake experiments; unexposed $\text{PM}_{2.5}$ filter which has not been used for any experiments.

Table 2. Summary of the collected mass and effective surface area of PM_{2.5} on the filter, and its ambient average mass concentrations on haze and non-haze days.

Samples	Weather	M _a (mg)	Concentration (μg m ⁻³)	A _{es} (cm ²)
Jul 31 ^a	haze	1.28	127.0	12.88
Jul 31 ^b	haze	1.61	156.9	13.75
Aug 01 ^a	haze	1.33	132.6	13.04
Aug 01 ^b	haze	1.39	136.7	13.19
Aug 02 ^a	haze	1.04	107.0	12.12
Aug 02 ^b	haze	1.39	137.8	13.21
Aug 03 ^a	haze→non-haze	0.60	61.7	10.09
Aug 03 ^b	non-haze	0.41	41.1	8.63
Aug 04 ^a	non-haze	0.10	9.2	3.15
Aug 04 ^b	non-haze	0.18	16.9	5.44
Aug 05 ^a	non-haze	0.26	25.6	6.85
Aug 05 ^b	non-haze	0.32	32.4	7.76

Note: ^a daytime; ^b nighttime; A_{es}, effective surface area; M_a, mass of PM_{2.5}.

Table 3. The uptake coefficients γ ($\times 10^{-4}$) of PAA on $PM_{2.5}$, ADS, and ATD under different relative humidity conditions. The values in the brackets are the lower limit of γ ($\times 10^{-5}$).

RH	$PM_{2.5h}$	$PM_{2.5n}$	ADS_l	ADS_h	ATD_l	ATD_h
3%	0.81 ± 0.26 (0.23 ± 0.06) ^a	0.98 ± 0.27 (0.54 ± 0.24) ^a	0.84 ± 0.01 (2.19 ± 0.27) ^b	1.37 ± 0.02 (1.72 ± 0.02) ^b	2.42 ± 0.02 (3.45 ± 0.03) ^b	1.86 ± 0.01 (0.93 ± 0.02) ^b
20%	1.37 ± 0.20 (0.40 ± 0.11) ^a	1.41 ± 0.38 (0.78 ± 0.33) ^a	1.26 ± 0.03 (3.27 ± 0.38) ^b	1.78 ± 0.03 (2.24 ± 0.04) ^b	2.15 ± 0.05 (3.07 ± 0.07) ^b	1.44 ± 0.03 (0.72 ± 0.05) ^b
40%	1.95 ± 0.52 (0.58 ± 0.24) ^a	1.99 ± 0.52 (1.11 ± 0.46) ^a	1.65 ± 0.08 (4.28 ± 0.5) ^b	2.11 ± 0.06 (2.66 ± 0.08) ^b	1.81 ± 0.03 (2.59 ± 0.04) ^b	1.27 ± 0.03 (0.64 ± 0.03) ^b
60%	2.76 ± 0.54 (0.83 ± 0.32) ^a	2.63 ± 0.70 (1.47 ± 0.63) ^a	2.26 ± 0.08 (5.86 ± 0.70) ^b	2.39 ± 0.04 (3.01 ± 0.06) ^b	1.62 ± 0.01 (2.31 ± 0.02) ^b	1.16 ± 0.02 (0.58 ± 0.01) ^b
75%	3.43 ± 0.63 (1.03 ± 0.38) ^a	3.42 ± 1.25 (1.92 ± 1.00) ^a	2.60 ± 0.03 (6.74 ± 1.25) ^b	2.55 ± 0.01 (3.21 ± 0.01) ^b	1.47 ± 0.01 (2.1 ± 0.002) ^b	1.07 ± 0.03 (0.53 ± 0.002) ^b
90%	4.20 ± 0.58 (1.24 ± 0.41) ^a	4.63 ± 1.30 (2.60 ± 1.09) ^a	3.21 ± 0.08 (8.32 ± 1.30) ^b	2.62 ± 0.01 (3.30 ± 0.01) ^b	1.17 ± 0.03 (1.67 ± 0.04) ^b	0.91 ± 0.04 (0.45 ± 0.03) ^b

Note: $PM_{2.5h}$, haze day $PM_{2.5}$; $PM_{2.5n}$, non-haze day $PM_{2.5}$; ADS_h and ATD_h , the mass of mineral dust about 1.3 mg; ADS_l and ATD_l , the mass of mineral dust about 0.3 mg; ^a uptake coefficient calculated by total surface area of the particles using size distribution, representing the lower limit; ^b uptake coefficient calculated by BET area, representing the lower limit; the errors represent the relative standard deviation between γ on particles of ascending and descending RH.

Table 4. Summary of the uptake coefficients of H₂O₂ on mineral dust particles in literature data.

Substrate	RH dependence	Uptake coefficient	Method	Reference
TiO ₂	N	$(1.53 \pm 0.11) \times 10^{-4} - (5.04 \pm 0.58) \times 10^{-4}$	AFT-CIMS	Pradhan et al. (2010a)
Gobi dust Saharan dust	P	$(3.33 \pm 0.26) \times 10^{-4} - (6.03 \pm 0.42) \times 10^{-4}$ $(6.20 \pm 0.22) \times 10^{-4} - (9.42 \pm 0.41) \times 10^{-4}$	AFT-CIMS	Pradhan et al. (2010b)
Al ₂ O ₃	N	$(1.21 \pm 0.04) \times 10^{-8} - (0.76 \pm 0.09) \times 10^{-7}$	T-FTIR	Zhao et al. (2011b)
SiO ₂	N	$(1.55 \pm 0.14) \times 10^{-8} - (0.61 \pm 0.06) \times 10^{-7}$	T-FTIR	Zhao et al. (2011a)
HNO ₃ -Al ₂ O ₃	N (<75%); P (>75%)	$\gamma_{\text{aged}}/\gamma_{\text{pristine}} = 0.5 - 1.1$	T-FTIR	Zhao et al. (2011a)
SO ₂ -Al ₂ O ₃	P	$\gamma_{\text{aged}}/\gamma_{\text{pristine}} = 1.2 - 1.9$	T-FTIR	Zhao et al. (2011a)
SiO ₂ Al ₂ O ₃ Fe ₂ O ₃ MgO	—	$\gamma_0 = (5.22 \pm 0.9) \times 10^{-5}$ $\gamma_0 = (1.00 \pm 0.11) \times 10^{-4}$ $\gamma_0 = (9.70 \pm 1.95) \times 10^{-5}$ $\gamma_0 = (1.66 \pm 0.23) \times 10^{-4}$	Knudsen cell-QMS	Wang et al. (2011)
TiO ₂	N	$\gamma_{0,\text{dark}} = \frac{4.1 \times 10^{-3}}{1 + \text{RH}^{0.65}}$	CWFT-QMS	Romanias et al. (2012)
SiO ₂ CaCO ₃	—	$\gamma_0 = \frac{\exp(934.5/T - 12.7)}{1 + \exp(934.5/T - 12.7)}$ $\gamma_0 = \frac{\exp(1193.0/T - 11.9)}{1 + \exp(1193.0/T - 11.9)}$	Knudsen cell-QMS	Zhou et al. (2012)
HNO ₃ -CaCO ₃	P	$\gamma_{\text{aged}}/\gamma_{\text{pristine}} = 1 - 8$	T-FTIR	Zhao et al. (2013)
SO ₂ -CaCO ₃	P	$\gamma_{\text{aged}}/\gamma_{\text{pristine}} = 3 - 10$	T-FTIR	Zhao et al. (2013)
Al ₂ O ₃ Fe ₂ O ₃	N N	$\gamma_0 = \frac{1.10 \times 10^{-3}}{1 + \text{RH}^{0.95}}$ $\gamma_0 = \frac{1.05 \times 10^{-3}}{1 + \text{RH}^{0.75}}$	CWFT-QMS	Romanias et al. (2013)
TiO ₂	N	$\gamma_0 = \frac{4.8 \times 10^{-4}}{1 + \text{RH}^{0.66}}$	CWFT-QMS	El Zein et al. (2014)

Note: N, negative RH dependence; P, positive RH dependence; γ_0 , initial uptake coefficient; AFT, aerosol flow tube; CIMS, chemical ionization mass spectrometer; T-FTIR, transmission-Fourier Transform Infrared spectroscopy; QMS, quadrupole mass spectrometer; CWFT, coated-wall flow tube.

Table 5. The average concentration of ions, organic acids and elements of PM_{2.5} on haze and non-haze days. The errors represent the relative standard deviation.

Species	haze day	non-haze day
SO ₄ ^{2-a}	42.3±7.88	5.95±5.88
NO ₃ ^{-a}	23.2±16.8	3.18±2.92
Cl ^{-a}	1.07±1.48	0.15±0.12
NH ₄ ^{+a}	6.11±1.22	1.51±1.01
K ^{+a}	1.10±0.27	0.26±0.16
Na ^{+a}	0.49±0.15	0.24±0.11
HO(O)CC(O)OH ^a	0.83±0.06	0.21±0.10
HC(O)OH ^a	0.20±0.09	0.07±0.06
CH ₃ C(O)OH ^a	0.19±0.16	0.16±0.32
CH ₃ C(O)C(O)OH ^a	0.04±0.01	0.01±0.01
Al ^a	0.45±0.36	0.10±0.09
Ca ^a	0.44±0.16	0.30±0.14
Mg ^a	0.10±0.04	0.05±0.03
P ^a	0.19±0.12	0.14±0.19
Fe ^a	0.60±0.14	0.17±0.10
Ti ^a	0.04±0.01	0.03±0.03
Mn ^a	0.03±0.01	0.01±0.01
Cu ^a	0.03±0.02	0.01±0.01
Zn ^a	0.18±0.08	0.03±0.02
V ^a	0.01±0.01	0.01±0.01
Pb ^a	0.08±0.02	0.01±0.01
Ba ^b	10.22±3.06	3.68±1.76
Cr ^b	8.55±2.58	4.16±2.49
Se ^b	4.56±1.60	1.28±0.95
Ni ^b	4.54±1.88	0.44±0.30
As ^b	4.30±2.64	5.57±3.63
Mo ^b	1.16±0.50	0.42±0.20
Tl ^b	1.12±0.41	0.14±0.10
Cd ^b	1.09±0.32	0.22±0.17
Co ^b	0.40±0.10	0.19±0.08
U ^b	0.04±0.01	0.02±0.02
Th ^b	0.03±0.02	0.01±0.02

Note: ^a the unit is $\mu\text{g m}^{-3}$; ^b the unit is ng m^{-3} .

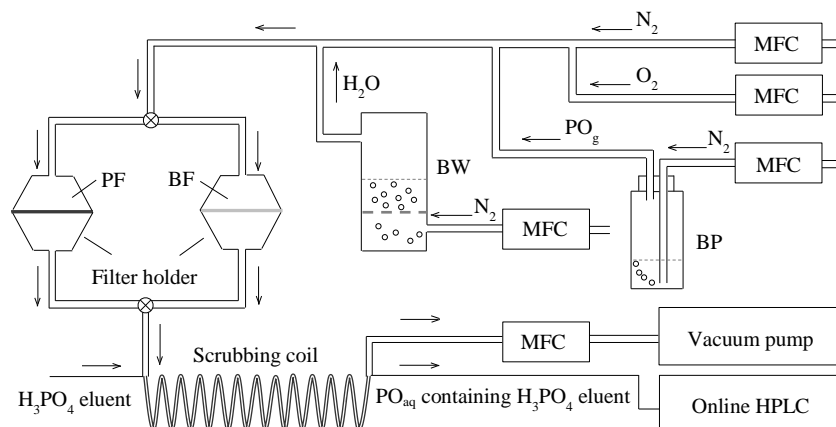


Fig. 1. Schematic diagram of experimental apparatus. MFC, mass flow controller; PF, particle-loaded filter; BF, blank filter; PO_g , gaseous peroxide compound; BP, bubbler for peroxide vapor; BW, bubbler for water vapor; HPLC, high-performance liquid chromatography. The scrubbing coil, BP and BW were kept in 277 K and 298 K water bath, respectively.

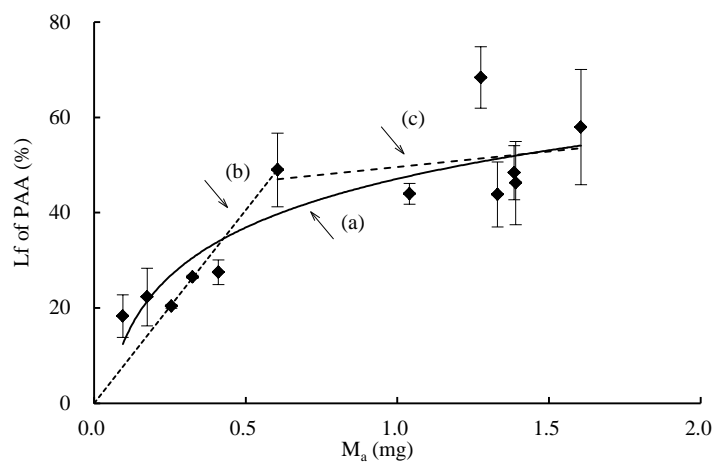


Fig. 2. The trend line of fractional loss (Lf) of PAA against $PM_{2.5}$ mass (M_a) (60% RH). Error bars are 1 standard deviation. Solid line (a), the logarithmic trend line of Lf against M_a among all mass values; dotted line (b), the linear correlation of Lf against M_a in the low mass region; dotted line (c), the nearly constant Lf against M_a in the high mass region.

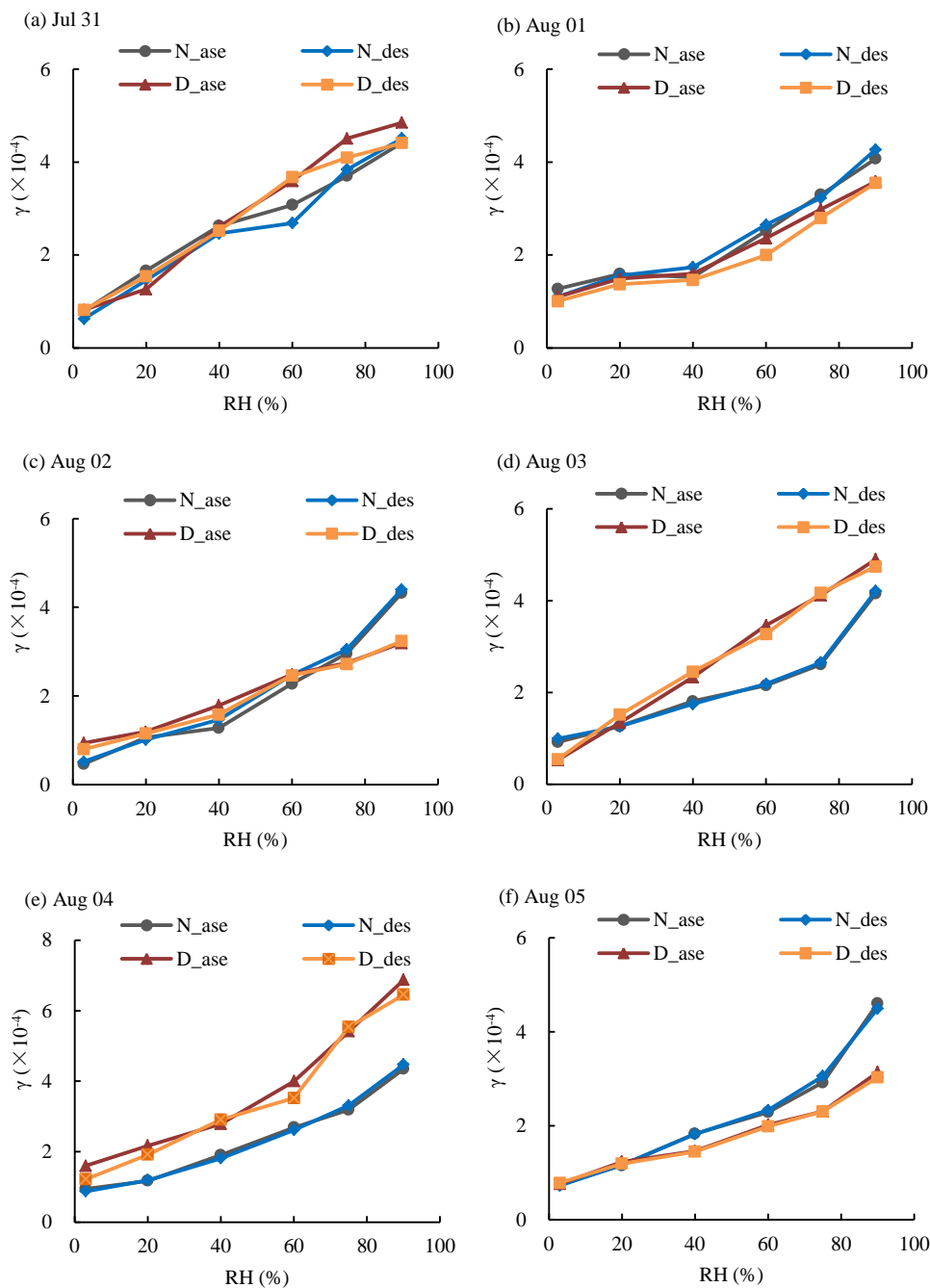


Fig. 3. Profiles of uptake coefficient of gaseous PAA on $PM_{2.5}$ over a range of RH (3–90%); N_{ase} , γ_{PAA} was measured with ascending RH on nighttime $PM_{2.5}$ particles; N_{des} , γ_{PAA} was measured with descending RH on nighttime $PM_{2.5}$ particles; D_{ase} , γ_{PAA} was measured with ascending RH on daytime $PM_{2.5}$ particles; D_{des} , γ_{PAA} was measured with descending RH on daytime $PM_{2.5}$ particles.

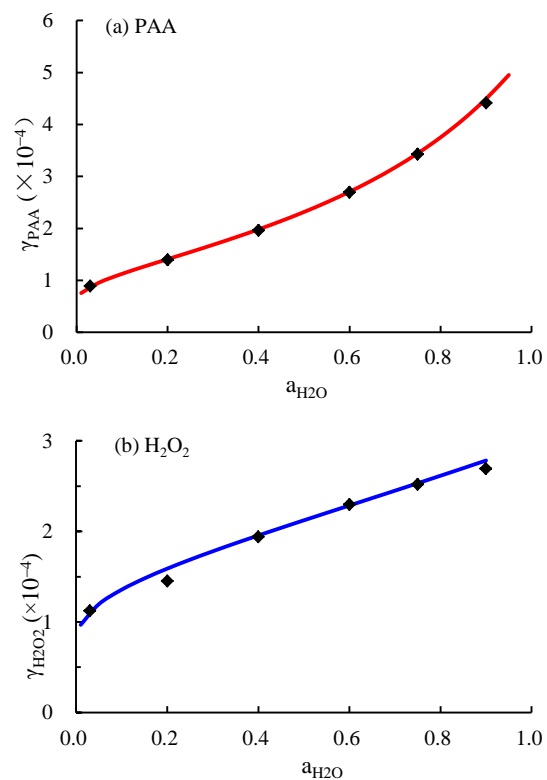


Fig. 4. The uptake coefficients of PAA and H₂O₂ on PM_{2.5} particles. The red line and the blue line in figure (a) and (b) represent the empirical fit of γ_{PAA} and $\gamma_{\text{H}_2\text{O}_2}$, respectively.

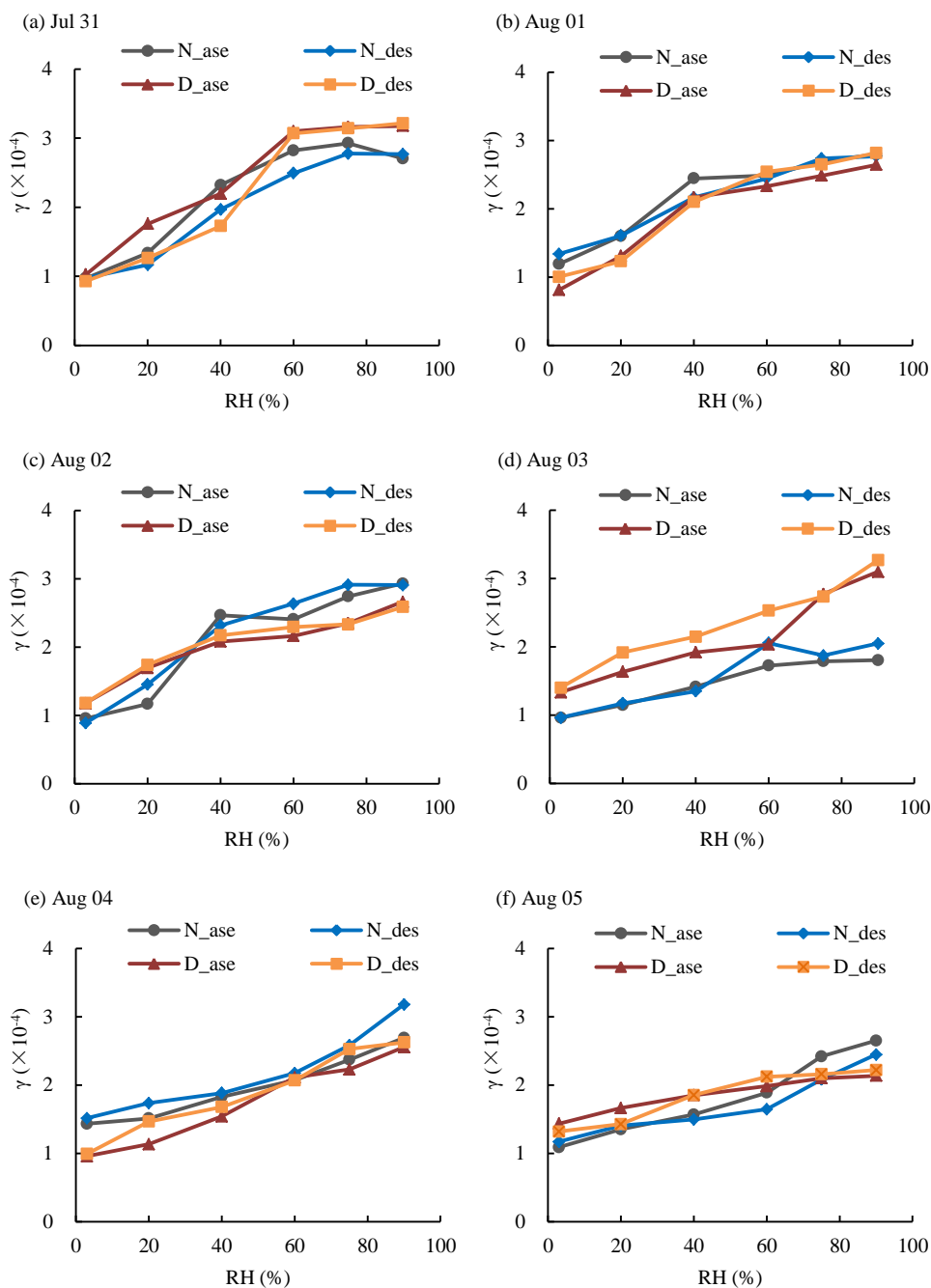


Fig. 5. Profiles of uptake coefficient of gaseous H_2O_2 on $PM_{2.5}$ over a range of RH (3–90%); N_{ase} , $\gamma_{H_2O_2}$ was measured with ascending RH on nighttime $PM_{2.5}$ particles; N_{des} , $\gamma_{H_2O_2}$ was measured with descending RH on nighttime $PM_{2.5}$ particles; D_{ase} , $\gamma_{H_2O_2}$ was measured with ascending RH on daytime $PM_{2.5}$ particles; D_{des} , $\gamma_{H_2O_2}$ was measured with descending RH on daytime $PM_{2.5}$ particles.

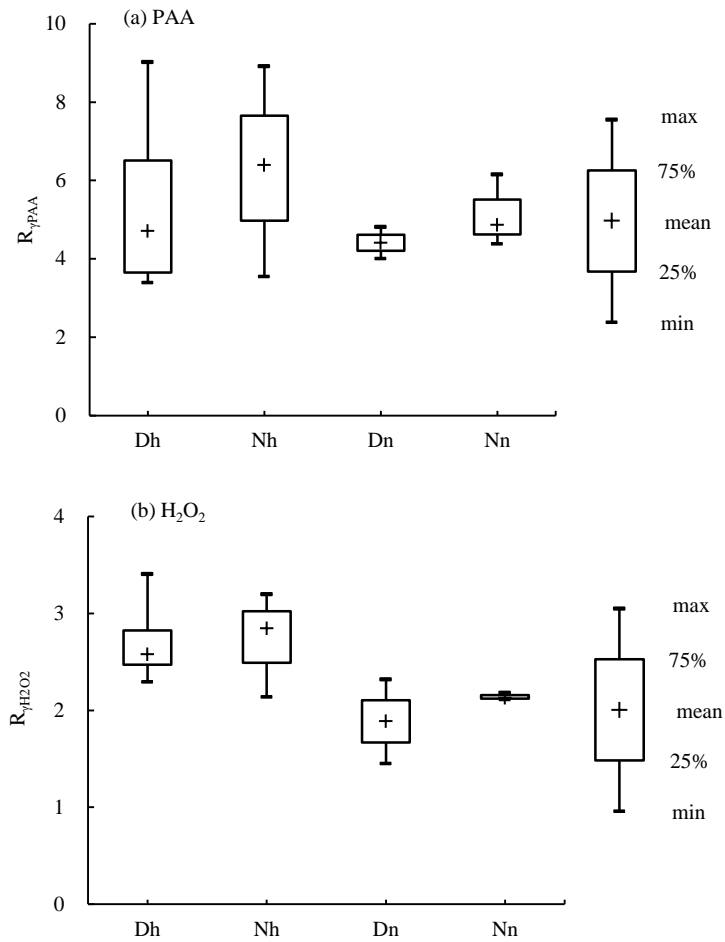


Fig. 6. The ratio of γ at 90% RH to γ at 3% RH ($R_{\gamma\text{PAA}}$ and $R_{\gamma\text{H}_2\text{O}_2}$) on $\text{PM}_{2.5}$. Dh, daytime of haze day; Nh, nighttime of haze day; Dn, daytime of non-haze day; Nn, nighttime of non-haze day.

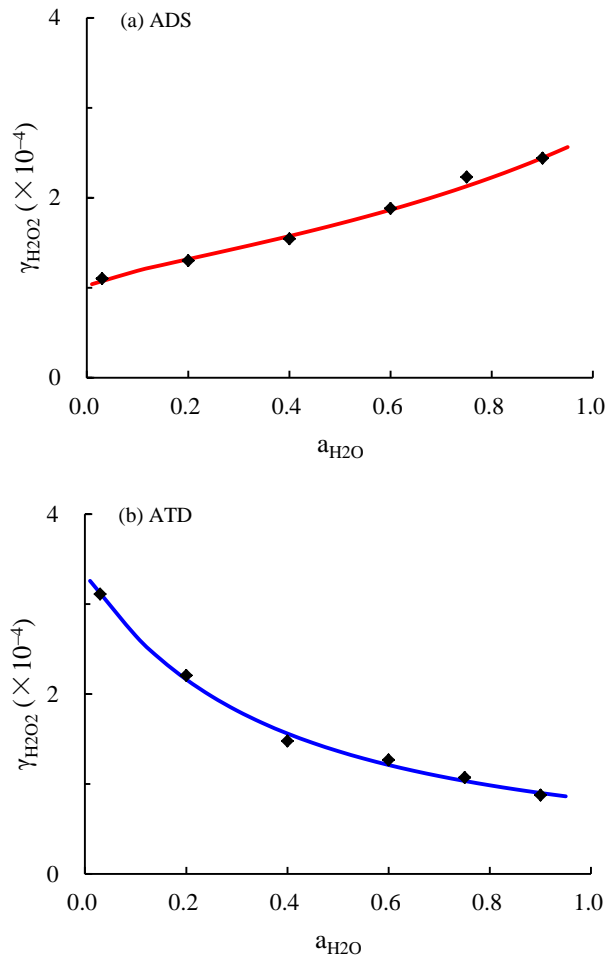


Fig. 7. Uptake coefficient of H_2O_2 on ADS and ATD particles. The red line and the blue line in figure (a) and (b) represent the empirical fit of $\gamma_{\text{H}_2\text{O}_2}$ on ADS and ATD particles, respectively.